# ORIGINAL RESEARCH

Peroxidasin Deficiency Re-programs Macrophages Toward Pro-fibrolysis Function and Promotes Collagen Resolution in Liver

Mozhdeh Sojoodi,[1] Derek J. Erstad,[1] Stephen C. Barrett,[1] Shadi Salloum,[2] Shijia Zhu,[3] Tongqi Qian,[3] Selene Colon,[4] Eric M. Gale,[5] Veronica Clavijo Jordan,[5] Yongtao Wang,[1] Shen Li,[1] Bahar Ataeinia,[5] Sasan Jalilifiroozinezhad,[6] Michael Lanuti,[7] Lawrence Zukerberg,[8] Peter Caravan,[5] Yujin Hoshida,[3] Raymond T. Chung,[2] Gautam Bhave,[8] Georg M. Lauer,[2] Bryan C. Fuchs,[1,*] and Kenneth K. Tanabe[1,*]

[1]Division of Gastrointestinal and Oncologic Surgery, Massachusetts General Hospital, Harvard Medical School, Boston, Massachusetts; [2]Liver Center, Division of Gastroenterology, Massachusetts General Hospital and Harvard Medical School, Boston, Massachusetts; [3]Liver Tumor Translational Research Program, Simmons 22 Comprehensive Cancer Center, Division of Digestive and Liver Diseases, Department of Internal Medicine, University of Texas Southwestern Medical Center, Dallas, Texas; [4]Division of Nephrology and Hypertension, Vanderbilt University Medical Center, Nashville, Tennessee; [5]Athinoula A. Martinos Center for Biomedical Imaging, Institute for Innovation in Imaging (i3), Department of Radiology, Massachusetts General Hospital, Harvard Medical School, Boston, Massachusetts; [6]Koch Institute for Integrative Cancer Research, MIT, Cambridge, Massachusetts; [7]Division of Thoracic Surgery, Massachusetts General Hospital Cancer Center, Harvard Medical School, Boston, Massachusetts; and the [8]Department of Pathology, Massachusetts General Hospital, Harvard Medical School, Boston, Massachusetts.
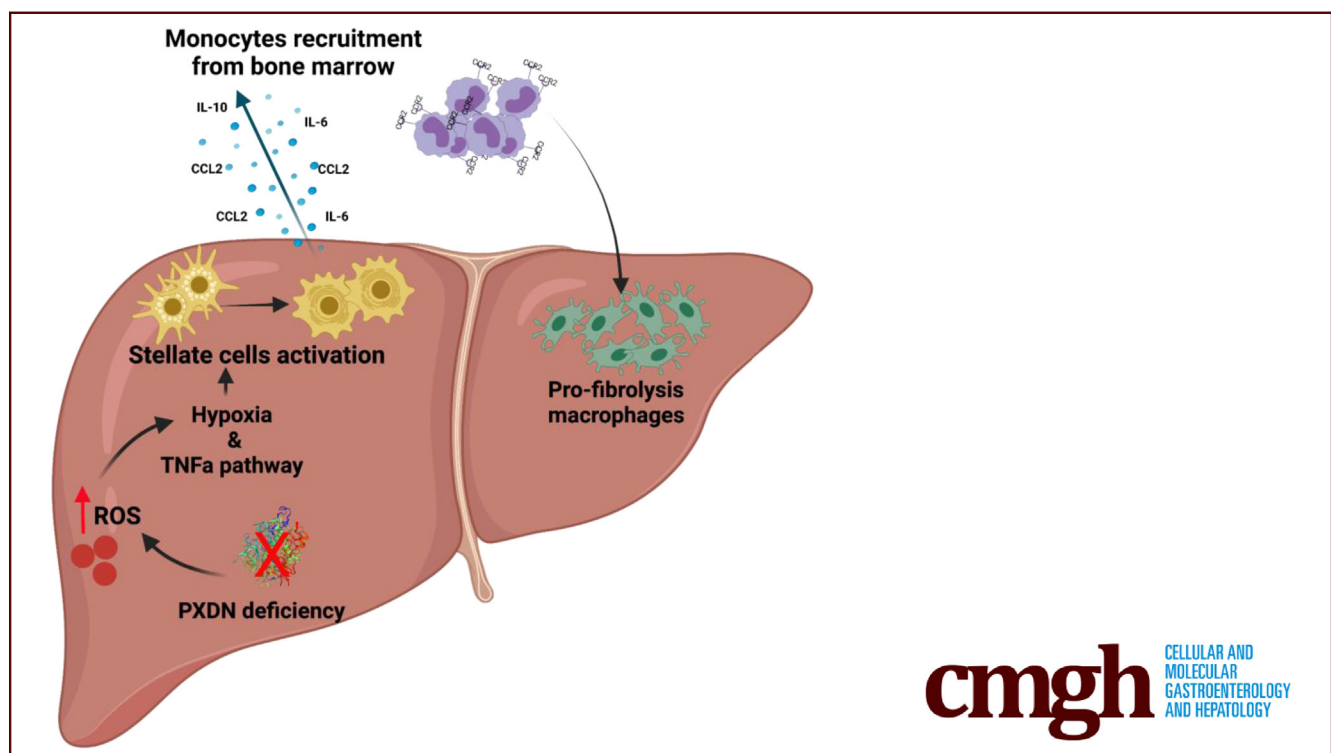
SUMMARY

Peroxidasin deficiency results in mild-hypoxic liver micro-environment and causes recruitment of monocytes and pro-fibrolysis macrophages in early stages of liver fibrosis. These events accelerate the resolution of fibrosis and organ healing.

BACKGROUND & AIMS: During liver fibrosis, tissue repair mechanisms replace necrotic tissue with highly stabilized extracellular matrix proteins. Extracellular matrix stabilization influences the speed of tissue recovery. Here, we studied the expression and function of peroxidasin (PXDN), a peroxidase that uses hydrogen peroxide to cross-link collagen IV during liver fibrosis progression and regression.

METHODS: Mouse models of liver fibrosis and cirrhosis patients were analyzed for the expression of PXDN in liver and serum. *Pxdn*^{-/-} and *Pxdn*^{+/+} mice were either treated with carbon tetrachloride for 6 weeks to generate toxin-induced fibrosis or fed with a choline-deficient L-amino acid-defined high-fat diet for 16 weeks to create nonalcoholic fatty liver disease fibrosis. Liver histology, quantitative real-time polymerase chain reaction, collagen content, flowcytometry and immunostaining of immune cells, RNA-sequencing, and liver function tests were analyzed. In vivo imaging of liver reactive oxygen species (ROS) was performed using a redox-active iron complex, Fe-PyC3A.

RESULTS: In human and mouse cirrhotic tissue, PXDN is expressed by stellate cells and is secreted into fibrotic areas. In patients with nonalcoholic fatty liver disease, serum levels of PXDN increased significantly. In both mouse models of liver fibrosis, PXDN deficiency resulted in elevated monocyte and pro-fibrolysis macrophage recruitment into fibrotic bands and caused decreased accumulation of cross-linked collagens. In *Pxdn*^{-/-} mice, collagen fibers were loosely organized, an atypical phenotype that is reversible upon macrophage depletion. Elevated ROS in *Pxdn*^{-/-} livers was observed, which can result in activation of hypoxic signaling cascades and may affect signaling pathways involved in macrophage polarization such as TNF-a via NF-kB. Fibrosis resolution in *Pxdn*^{-/-} mice was associated with significant decrease in collagen content and improved liver function.

CONCLUSION: PXDN deficiency is associated with increased ROS levels and a hypoxic liver microenvironment that can regulate recruitment and programming of pro-resolution macrophages. Our data implicate the importance of the liver microenvironment in macrophage programming during liver fibrosis and suggest a novel pathway that is involved in the resolution of scar tissue. (*Cell Mol Gastroenterol Hepatol 2022;13:1483–1509;* https://doi.org/10.1016/j.jcmgh.2022.01.015)

Liver fibrosis is a byproduct of dysregulated wound healing in response to chronic hepatic injury.[1] It is characterized by excessive extracellular matrix (ECM) deposition resulting in dense scarring that impairs normal liver structure and physiology over time. Cirrhosis, the end-stage of liver fibrosis, is the ninth leading cause of death in the United States and imposes a substantial health crisis globally. This burden has increased worldwide since 1990.[2]

Although the consequences of cirrhosis and end-stage liver failure have been well-characterized, the mechanism of scar formation in response to injury is less well understood.[3] Inflammatory signaling is central to the process of acute hepatic injury and influences the wound healing response.[4] Degenerating hepatocytes release pro-inflammatory damage response signals that chemotactically recruit immune cells and stimulate activation of quiescent hepatic stellate cells (HSCs).[1] Activated HSCs have been implicated as the primary producer of ECM during liver wound healing. They secrete chemotactic signals to recruit circulating monocytes and tissue-resident macrophages, known as Kupffer cells, to the site of injury.[5] Kupffer cells are located inside in the space of Disse alongside HSCs and patrol the sinusoids. Signals sent from activated stellate cells and injured hepatocytes activate macrophages and trigger their innate immune response.[6] Activated resident macrophages and HSCs secrete cytokines and growth factors, such as CCL2, to recruit monocytes from bone marrow.[7] In the hepatic microenvironment, recruited monocytes mature into macrophages following local reprogramming to either deteriorate immune system responses and drive fibrosis,[7,8] or resolve the deposited ECM and maintain tissue integrity.[9]

Activated macrophages are thought to play a critical role in mediating the acute inflammatory process of hepatic injury and subsequent fibrotic response.[10] Historically, macrophages have been classified as pro-inflammatory M1 (CD11c^{+}) or pro-healing M2 (CD206^{+}) populations. However, in recent years, it has become clear that there is greater complexity among macrophages, and they have to be characterized based on their origins, activation signals, and functions.[11,12] Notably, M2 macrophages have been shown to promote normal tissue repair by suppressing inflammation, promoting ECM degradation, and deactivating myofibroblasts, thus having an anti-fibrotic impact.[13] Conversely, M1 macrophages are thought to drive aberrant HSC activation, resulting in excessive scar formation.[14] Tissue redox states are thought to influence the dynamic of M1/M2 macrophage phenotypes.[15,16]

In this study, we investigated peroxidasin (PXDN), a heme-containing peroxidase that is highly conserved in the animal kingdom and catalyzes the oxidation of various substrates in the presence of H2O2. *Pxdn* participates in ECM formation by cross-linking collagen type IV formation of sulfilimine bonds.[17] PXDN is mainly expressed in endothelial cells, epithelial cells, and fibroblasts.[18,19] In both humans and rodents, genetic mutation in the *Pxdn* gene interrupts cross-linking of collagen IV and leads to anterior segment dysgenesis of the eyes, congenital cataracts, corneal opacity, and glaucoma.[20-22] PXDN is present in the

Most current article

endoplasmic reticulum of human primary pulmonary, dermal, and kidney fibroblasts, and expression of this protein is increased during transforming growth factor-β1 (TGF-b)-induced myofibroblast activation.[18,23,24] PXDN expression and function in healthy and diseased liver have not been reported yet and, given this context, we sought to characterize PXDN expression in healthy liver and in response to injury and scar formation.

Results

PXDN Expression is Upregulated During Liver Fibrosis and PXDN Deficiency Induces Stronger Activation of Stellate Cells Without Affecting Collagen Production

PXDN expression in myofibroblasts is upregulated during dermal, cardiac, and kidney fibrosis.[18,25,26] Based on the single-cell RNA sequencing data set published by Ramachandran et al, PXDN is exclusively expressed in the endothelia and fibroblasts of normal and cirrhotic liver.[19] To better study the expression pattern of PXDN during liver fibrosis, we performed immunofluorescent staining on human healthy and cirrhotic livers for PXDN and smooth muscle actin (SMA or ACTA2, a marker of activated HSCs). In healthy liver, we observed PDXN staining in myofibroblasts (ACTA2-positive cells) surrounding normal appearing vasculature (Figure 1, A). Conversely, in cirrhotic liver, PDXN staining was prominent in proximity to HSCs in bands of fibrosis surrounding the regenerative nodules, as assessed by co-staining for ACTA2 (Figure 1, A). We also investigated serum levels of PXDN in healthy and cirrhotic patients. Subjects were considered cirrhotic based on their pathology report and fibrosis score (F3-4) reported by an expert pathologist. Information about age, gender, and etiology of cirrhosis patients is listed in Table 1. Serum PXDN was significantly higher in cirrhosis patients compared with healthy controls (27.1 $\pm$ 16.77 vs 2.01 $\pm$ 1.5 ng/mL; $P <$ .001) (Figure 1, B). To determine whether HSCs produce PXDN, we activated primary human HSCs with TGF-b in vitro and measured ACTA2 and PXDN mRNA and protein expression before and after HSCs activation. In response to TGF-b, HSCs lose their vitamin A-storing oil droplets, stained by oil red, and upregulate *Acta2* and *Pxdn* (Figure 1, C-D). In addition, we observed an increase in the level of secreted PXDN in the conditioned medium collected from activated HSCs in vitro (Figure 1, E).

Next, we used a carbon tetrachloride (CCl4) hepatic injury model in mice to induce liver fibrosis. In this model, repeated injections of CCl4 for 6 weeks (3× per week) led to robust hepatotoxicity, inflammation, HSC activation, and ECM deposition. The vehicle control group received olive oil for 6 weeks (3× per week). We examined livers in early (3 weeks) and late stages (6 weeks) of liver fibrosis in these mice (Figure 1, E). Expression of *Acta2*, *Col1a1*, and *Pxdn* peaked at 3 weeks post CCl4 injection, whereas at 6 weeks, fibrosis is well-established, and expression of these genes was reduced to baseline levels (Figure 1, F-H). In mouse cirrhotic liver tissue, PXDN was also present in fibrotic regions of liver and co-localized with ACTA2 (Figure 1, H).

Taken together, our data show that activated HSCs produce and secrete PXDN, with increased PXDN expression in injured and cirrhotic livers in regions of active tissue fibrosis.

Next, we investigated whether PXDN contributes to scar formation in injured mouse livers. We measured fibrosis development in *Pxdn* deficient (*Pxdn$^{-/-}$*) mice compared with their *Pxdn$^{+/+}$* (*Pxdn$^{+/+}$*) littermates after repeated administration of CCl4 for 3 or 6 weeks. Sirius red (SR) staining of collagen revealed that collagen proportional area as well as total liver collagen content, measured by hydroxyproline assay, were not significantly different between *Pxdn$^{-/-}$* and *Pxdn$^{+/+}$* mice at both timepoints (Figure 2, A-C). mRNA expression of collagen types I, III, and IV did not change at both time points between *Pxdn$^{-/-}$* and *Pxdn$^{+/+}$* livers (Figure 2, D-F). In summary, PXDN deficiency does not affect collagen expression and deposition during murine liver fibrosis.

PXDN Deficiency is Associated With Abnormal Collagen Fiber Formation

Although collagen quantity changed little in the absence of PXDN, the morphology of collagen fiber was altered in *Pxdn$^{-/-}$* mice. Fibrotic bands in *Pxdn$^{-/-}$* mice had wider septae (~2-fold increase at 3 weeks and ~3-fold increase at 6 weeks of CCl4 administration), and collagen fibrils were loosely organized into a single fiber bundle (Figure 3, A-B). The main constituent of fibrotic tissue in liver fibrosis is fibril-forming collagens, such as collagen type 1 (COL1).[27] Immunofluorescent staining of COL1 suggests that improper organization of COL1 fibers contributes to disorganized fiber bundles in *Pxdn$^{-/-}$* liver (Figure 3, C). In addition, high-resolution scanning electron microscopy (SEM) of liver tissue showed the parallel arrangement of fibrils with the typical banded pattern of collagen fibers in *Pxdn$^{+/+}$* cirrhotic livers are absent in *Pxdn$^{-/-}$* livers (Figure 3, D).

Alteration in collagen fiber formation can reduce the ECM stabilization and change the milieu of fibrotic tissue.[28] To examine ECM stabilization, we compared the percentage of collagen with the different levels of stability in *Pxdn$^{-/-}$* and *Pxdn$^{+/+}$* livers after 6 weeks of CCl4 administration. At the advanced stage of liver fibrosis (6 weeks post CCl4), the proportion of newly synthesized collagens did not change in *Pxdn$^{-/-}$* mice; however, moderately cross-linked collagens (pepsin-soluble fraction) increased significantly from 52% in the *Pxdn$^{+/+}$* group to 76% in the *Pxdn$^{-/-}$* group. Concurrently, the fraction of highly cross-linked collagen decreased from 48% in the *Pxdn$^{+/+}$* group to 21% in the *Pxdn$^{-/-}$* group (Figure 3, E). These data suggest that PXDN deficiency is associated with altered collagen fiber stabilization during liver fibrosis.

PXDN has been reported to mediate collagen type IV cross-linking through the formation of sulfilimine bonds.[29] Collagen IV is not one of the major collagens contributing to fibrotic scar formation in the liver, but due to the established role of PXDN in collagen cross-linking, we examined whether the deficiency of PXDN during liver fibrosis could result in collagen bundle formation. By
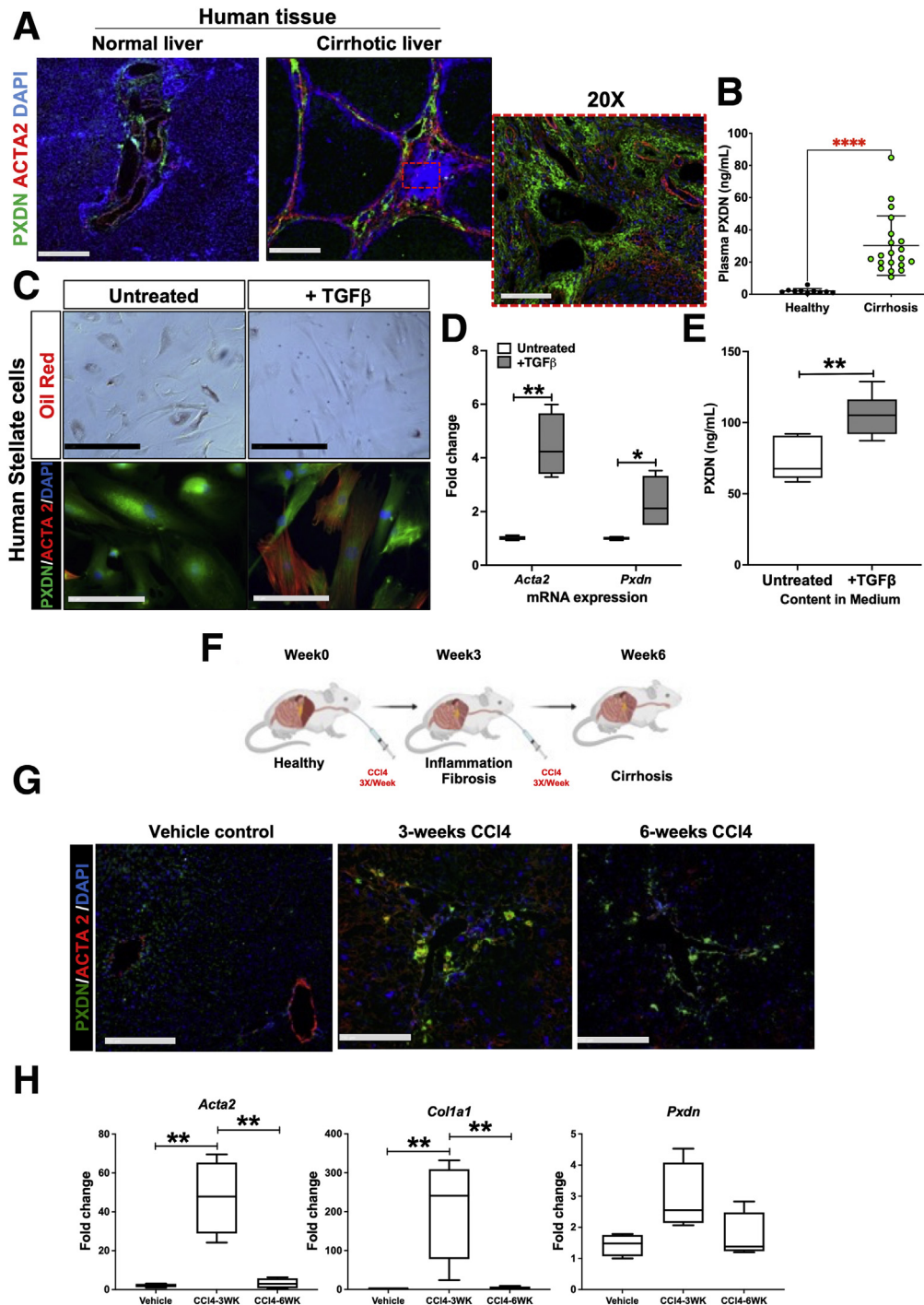
Figure 1. PXDN is upregulated in human and mouse cirrhotic liver tissue. *A*, Co-immunostaining of PXDN with smooth muscle actin (ACTA2) and DAPI in healthy human liver and cirrhotic patient. Higher magnification shows intra and extra-cellular expression of PXDN in fibrotic area in cirrhotic liver. Scale bars = 250 mm on 10× pictures of normal and cirrhotic livers and 100 mm on magnified (20×) picture of cirrhotic liver (*in dotted red box*). *B*, PXDN serum analysis of 10 healthy individuals and 20 cirrhotic patients (mean ± standard deviation, Student *t* test, ****$P <$ .0001). *C*, Human primary stellate activation after TGF-b treatment is visualized with Oil Red O staining and co-immunostaining of PXDN with smooth muscle actin (ACTA2) and DAPI. Scale bars = 250 mm. *D*, mRNA expression of *Acta2* and *Pxdn* after TGF-b (20 ng/mL) induction (n = 4, mean ± standard deviation, Multiple *t*-test, *$P <$ .05, **$P <$ .01). *E*, PXDN protein content in the medium after stellate cells activation with TGF-b (20 ng/mL) (n = 4, mean ± standard deviation, Student *t* test, **$P <$ .01). F, To induce liver cirrhosis in experimental animal model, mice received CCl4, 3× per week via oral gavage for 6 weeks. Vehicle control animals received olive oil via gavage (*G, H*) *Acta2, Col1a1* mRNA, and protein expression during the development of liver cirrhosis in CCl4 mouse model. Scale bars = 250 mm. (n = 4, mean ± standard deviation, Multiple *t* test, **$P <$ .01).

Table 1. Age, Gender, Etiology, and PXDN Serum Level of Patients With Cirrhosis

	Healthy	Cirrhosis	P-value
Number of values	10	20	
Gender			
Male	6 (60%)	11 (55%)	.2
Female	4 (40%)	9 (45%)	
Age, y			
Average	34 ± 6	58 ± 10	< .0001
Minimum	25	39	
Maximum	40	76	
Etiology			
NASH	NA	9	
ALD	NA	11	
PXDN level, ng/mL			
Minimum	0.5	11	
Maximum	6	85	
Range	5	74	
Mean	2	27	< .0001
Standard deviation	1	17	

ALD, Alcoholic liver disease; *NA*, not applicable; *NAFLD*, nonalcoholic fatty liver disease; *NASH*, nonalcoholic steato-hepatitis; *PXDN*, peroxidasin.

quantification of sulfilimine cross-links, we observed that $Pxdn^{-/-}$ mice possess fewer collagen IV sulfilimine cross-links in healthy liver compared with their $Pxdn^{+/+}$ littermates. However, we did not detect any difference in collagen IV sulfilimine cross-linking between $Pxdn^{-/-}$ fibrotic and healthy livers (Figure 4, A-C). Therefore, we concluded that reduced collagen IV cross-links is not the cause of loose formation of collagen bundles in $Pxdn^{-/-}$.

PXDN Deficiency is Associated With Increased Macrophages Recruitment Into Liver

Hematoxylin and eosin (H&E)-stained liver tissue sections showed robust inflammatory infiltration in the livers of $Pxdn^{-/-}$ and $Pxdn^{+/+}$ mice at 3 and 6 weeks after repeated CCl4 injection (Figure 5). Due to the known role of macrophages in mediating immune response to liver injury, we further analyzed the changes in macrophage cell populations by multicolor flow cytometry. Gating strategy and differential expression of cell surface markers in each population are shown in Figure 6. Total population of monocytes (CD45$^+$CD11b$^+$) increased over the course of disease progression and was significantly higher in $Pxdn^{-/-}$ mice after 3 weeks of CCl4 injection compared with $Pxdn^{+/+}$ mice shown by CD11b immunostaining (Figure 7, A) and flow cytometry (47.3 ± 3.7 vs 34.2 ± 4.3; $P < .01$) (Figure 7, B). Hepatic macrophages (CD45$^+$ F4/80$^+$) are a heterogeneous cell population that includes both liver-resident and bone marrow-derived macrophages. Total hepatic macrophages were significantly increased in $Pxdn^{-/-}$ livers in vehicle controls (without injury) (16.9 ± 2.4 vs 12 ± 3.17; $P < .05$), after 3 weeks of CCl4 injection (37.3 ± 2.3 vs 23.3 ± 1; $P < .01$), and after 6 weeks of CC4 injection (44.5 ± 2.6 vs 39.0 ± 0.9; $P < .05$) compared with $Pxdn^{+/+}$ livers (Figure 7, C-D).

Classically activated (M1) macrophages primarily have pro-inflammatory and pro-fibrogenesis properties,[30] whereas alternatively activated (M2) macrophages are anti-inflammatory and promote tissue repair.[31] In healthy liver, there is a balance between M1 and M2 macrophages. Classically activated M1 macrophages are proinflammatory (CD45$^+$F4/80$^+$CD11c$^+$) and promote tissue injury and recruitment of macrophages as well as other immune cells to the site of injury. Alternatively activated M2 macrophages (CD45$^+$F4/80$^+$CD206$^+$) are known as healing macrophages and remodel/resolve ECM components and facilitate tissue repair.[32] We detected an increase in the percentage of M2 macrophages after 6 weeks of CCl4 injection in $Pxdn^{-/-}$ mice compared with $Pxdn^{+/+}$ mice (Figure 7, E-F) (27.2 ± 4.1 vs 19.1 ± 1.3; $P < .05$). The percentage of M1 macrophages remained similar at all time points (Figure 7, G).

Following injury, CCR2$^+$ monocytes are recruited from peripheral blood to injured liver to direct the initiation and resolution of inflammation that is essential for tissue repair. In our study, we detected a significant increase in the percentage of CCR2$^+$ macrophages in the $Pxdn^{-/-}$ mice after 3 weeks of CCl4 (54 ± 8.4 vs 34.7 ± 3.1; $P < .01$) (Figure 7, H). However, we did not detect a significant difference between Ly6C^{low} monocytes and Ly6C^{high} monocytes in $Pxdn^{-/-}$ mice vs $Pxdn^{+/+}$ mice during liver fibrosis progression (Figure 7, I-J). Taken together, we observed that in the early stage of the disease (3 weeks of CCl4), the population of macrophages is elevated in the $Pxdn^{-/-}$ livers, and at the later stage (6 weeks of CCl4), these macrophages take on a restorative phenotype (M2 or CD206$^+$) and recruit CCR2$^+$ macrophages from bone marrow.

Macrophages Participate in Fibrolysis From Early Stage of Fibrosis in Pxdn$^{-/-}$ Mice

Macrophages are the main sources of matrix metalloproteases (MMPs), which degrade ECM.[33] In particular, MMP8 (collagenase 2) and MMP13 (collagenase 3) are expressed by macrophages and neutrophils,[33] and their overexpression has been associated with significantly reduced liver fibrosis and enhanced hepatocyte proliferation.[34-36] Co-staining of collagen fibers (with SR staining) and macrophages (F4/80 immunohistochemistry [IHC]) in livers of CCl4 mice showed F4/80$^+$ cells are located in regions of fibrotic tissue in $Pxdn^{-/-}$ mice at both 3 and 6 weeks after repeated CCl4 injection (Figure 8, A). MMP8 and MMP13 protein expression was assessed by IHC and revealed that both MMP8 and MMP13 expression are more abundant in $Pxdn^{-/-}$ livers 6 weeks post CCl4 injection compared with $Pxdn^{+/+}$ livers (Figure 8, B). In addition, SEM images show a higher presence of immune cells in the fibrotic bands of $Pxdn^{-/-}$ livers at 6 weeks post CCl4 (Figure 8, C).

To further investigate the role of macrophages in fibrolysis reaction during liver injury in $Pxdn^{-/-}$ mice in vivo, we used a liposome mediated macrophage "suicide" approach to deplete macrophages.[37,38] $Pxdn^{-/-}$ mice were injured with CCl4 and then intravenously injected with 100 μL of clodronate-loaded liposome suspension (25 μg/gr
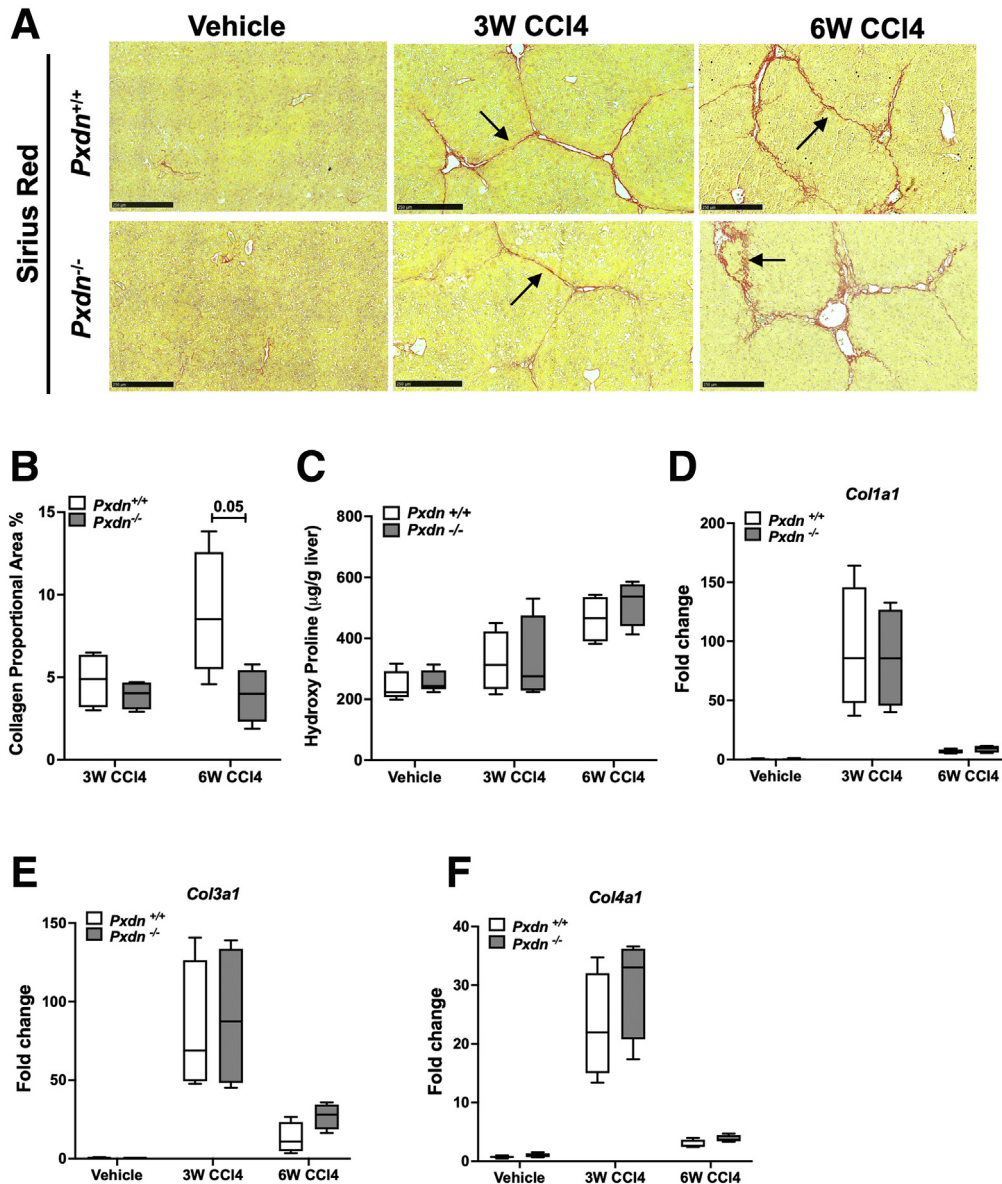
Figure 2. Collagen expression and deposition in $Pxdn^{-/-}$ mice. *A*, SR staining of collagen fibers. *Black arrows* show fibrotic bands after 3 and 6 weeks of CCl4 administration. Scale bar = 250 mm. *B*, Collagen proportional area (%) is the quantification of SR staining. *C*, Total liver collagen content is assessed by measuring hydroxyproline amino acid in the tissue and normalized to liver weight. *D-F*, mRNA expression analysis of *Col1a1*, *Col3a1*, and *Col4a1*.

mouse) once a week, starting after 3 weeks of CCL4 (Figure 8, *D*). Control $Pxdn^{-/-}$ CCl4 mice were injected with 100 μL control liposomes with the same schedule. Co-staining of macrophages (F4/80$^+$ cells) and collagen fibers showed that macrophages are significantly depleted from the liver after clodronate injection, and this depletion is associated with a reversion of the phenotype of disorganized collagen fibers seen in $Pxdn^{-/-}$ mice after 6 weeks of CCl4 injection (Figure 8, *E*). To induce recruitment of monocytes to the liver, we continued the injection of CCl4 for an additional week while clodronate was withdrawn. The goal of this experiment was to investigate whether recruited monocytes from bone marrow are able to differentiate and display the specific fibrolytic phenotype that was seen in $Pxdn^{-/-}$ resident macrophages prior to depletion. We observed that macrophage population, shown with IHC of F4/80 marker, is replenished, and these macrophages are

in close proximity and associated with collagen fibrils, as shown by SR staining (Figure 8, *F*). These data indicate that recruited monocytes differentiate to macrophages and acquire the unique fibrolytic phenotype seen in resident macrophages in $Pxdn^{-/-}$ livers.

During liver injury, bone marrow monocytes are recruited to the site of injury to boost macrophage population in liver.[39,40] Previous studies suggest that monocyte origin may not be the key determinant of macrophage identity, but rather the liver microenvironment ultimately determines the phenotype of the recruited cells.[41] To test whether $Pxdn^{-/-}$ liver microenvironment can affect differentiation of $Pxdn^{+/+}$ macrophage during liver injury, we sought to investigate the spatial distribution of monocytes isolated from $Pxdn^{-/-}$ and $Pxdn^{+/+}$ mice after intrahepatic transplantation into their opposite genotype. To establish cirrhosis, $Pxdn^{-/-}$ and $Pxdn^{+/+}$ mice were treated with CCl4

Figure 3. Morphology of fibrotic septae is significantly altered in *Pxdn*^{-/-} injured livers, with reduced accumulation of highly crosslinked, stable collagens in vivo. *A*, SR staining of collagen fibers. *Black arrows* mark the width of each fiber band. Scale bar = 50 mm. *B*, Width of collagen fibers increases during progression of liver fibrosis in *Pxdn*^{-/-} mice (n = 4 mice, mean ± standard deviation, 2-way analysis of variance, **P < .01). *C*, Immunostaining of Collagen I in *Pxdn*^{-/-} and *Pxdn*^{+/+} livers after 6 weeks of CCl4 injection. Scale bars = 250 mm on 20× pictures and 100 mm on magnified (40×) pictures (in *dotted red box*). *D*, Scanning electron microscopy of *Pxdn*^{+/+} and *Pxdn*^{-/-} fibrotic tissue. Typical banded pattern of collagen fibers in *Pxdn*^{+/+} livers (*red arrow*) is missing from *Pxdn*^{-/-} livers. *E*, Fibrotic matrix stability was measured in *Pxdn*^{-/-} and *Pxdn*^{+/+} livers after 6 weeks gavage with either vehicle or CCl4 via serial collagen extraction and hydroxyproline quantification in each fraction (salt-soluble, acid-soluble, pepsin-soluble, and insoluble collagen) (n = 3 mice, mean ± standard deviation, 1-way analysis of variance, *P < .05).
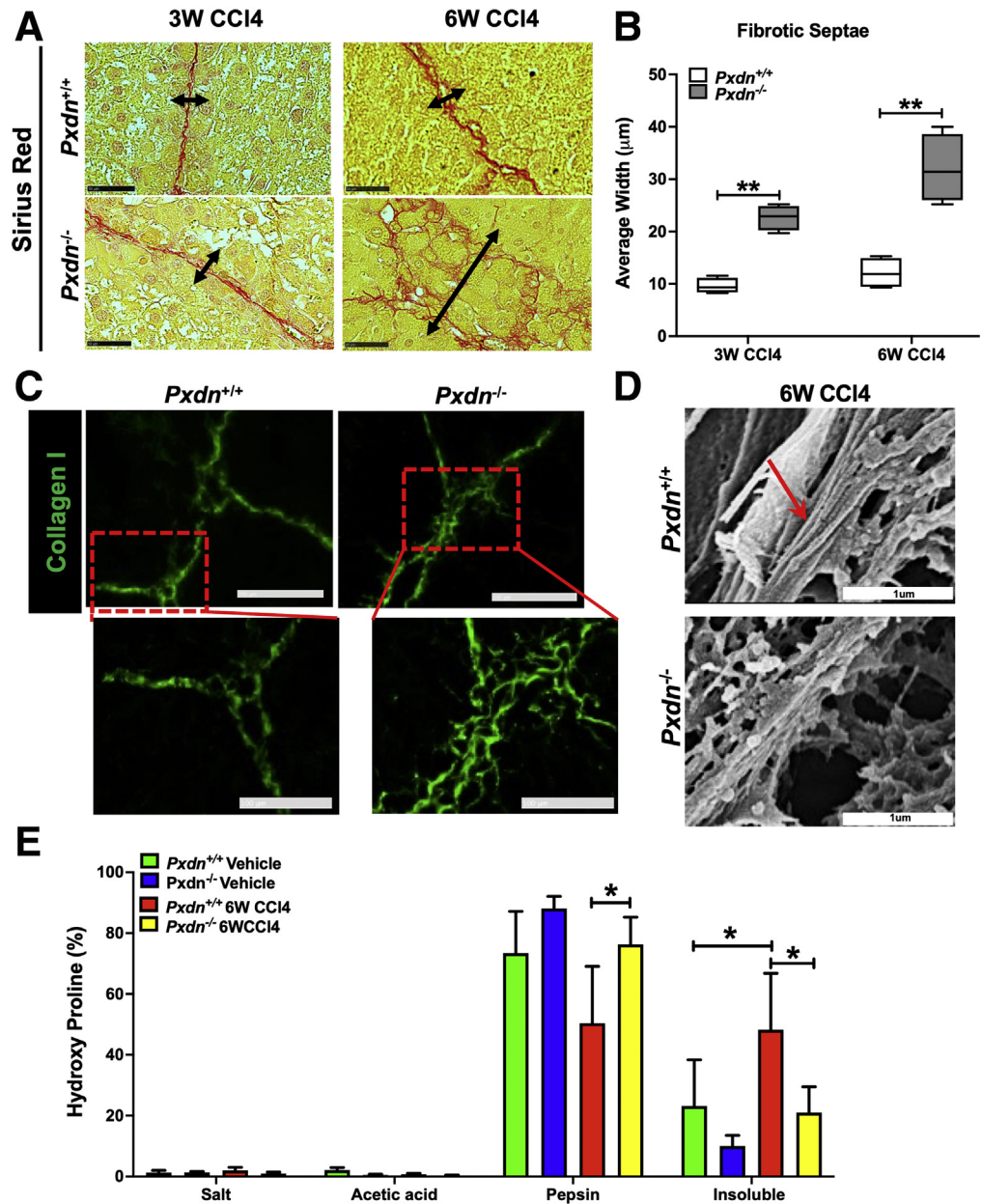
3 times weekly for 6 weeks. Bone marrow from the femur and tibia of healthy *Pxdn*^{-/-} and *Pxdn*^{+/+} mice was used as a source of monocytes for this experiment. Monocytes were harvested by flushing with Dulbecco's Modified Eagle's Medium (DMEM) supplemented with 1% fetal bovine serum (FBS). Cell suspension was supplemented with 20 nM macrophage-colony stimulating factor (M-CSF) and cultured on ultra-low attachment surfaces to avoid adhesion-triggered differentiation of monocytes for 24 hours. Liver resident macrophages were depleted with clodronate containing liposomes 24 hours prior to intrahepatic injection of primary monocytes. 10^6 primary monocytes were injected into the left lobe of liver. Mice were scarified 24 hours post-injection and liver tissue was collected for further analysis (Figure 8, *G*). Co-staining of macrophage marker (F4/80)

and collagen (SR) revealed that when *Pxdn*^{-/-} monocytes are injected into the *Pxdn*^{+/+} cirrhotic liver, they reside in the liver parenchyma and are not in the vicinity of fibrotic area. Conversely, *Pxdn*^{+/+} monocytes that were injected into *Pxdn*^{-/-} microenvironment are found near fibrotic bands (Figure 8, *H*). These data show the important role of the *Pxdn*^{-/-} liver microenvironment in programming of recruited (injected) macrophages during fibrosis progression.

PXDN Deficiency Accelerates Fibrosis Regression and Improves Liver Function

Decrease in collagen crosslinking and matrix stabilization accelerate the fibrolysis and reversal of liver fibrosis in *Pxdn*^{-/-} mice.[28] To investigate whether fibrosis regression in
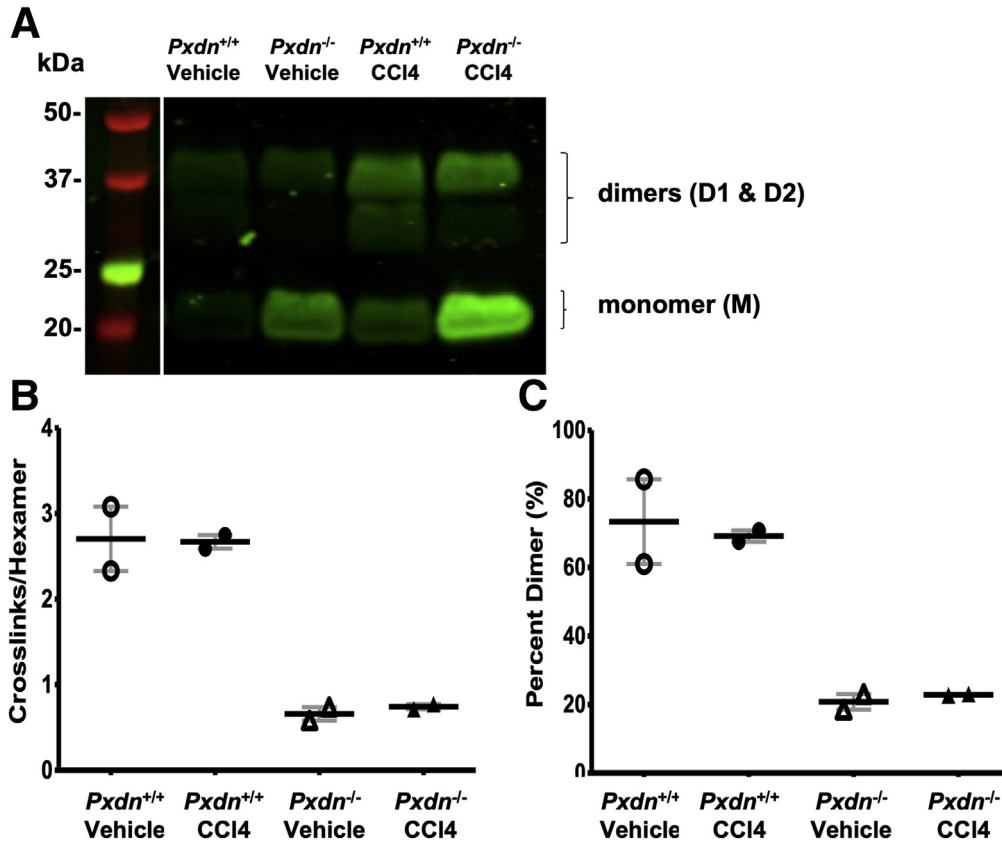
Figure 4. Collagen IV cross-linking in *Pxdn*^{-/-} and *Pxdn*^{+/+} livers before and after CCl4 injury. Sulfilimine cross-link content in *Pxdn*^{+/+} and *Pxdn*^{-/-} livers in healthy (Vehicle controls) and after CCl4 injury. *A*, Western blot after SDS-PAGE under non-reducing conditions of purified NC1 hexamers from *Pxdn*^{+/+} and *Pxdn*^{-/-} mice. Under denaturing conditions, collagen type IV hexamers dissociate into singly cross-linked dimeric (D1), doubly cross-linked dimeric (D2), and un-cross-linked monomeric (M) subunits. *B&C*, Number of sulfilimine cross-links per hexamer was quantified using densitometry of D1, D2, and M subunits for *Pxdn*^{+/+} and *Pxdn*^{-/-} mice. Individual data points (n = 2 mice) are displayed with mean ± standard deviation.

Pxdn^{-/-} liver is faster, we used a model of recovery from CCl4-induced fibrosis where CCl4 is injected for 6 weeks and then withdrawn for 4 weeks (Figure 9, *A*). After the 10 weeks, liver, spleen, and blood were collected for further analysis. Four weeks after discontinuation of CCl4, *Pxdn*^{-/-} liver had glossy surface and bright red color, whereas *Pxdn*^{+/+} liver still showed the fibrotic gross phenotype and liver color was pale (Figure 9, *B*). Serum aminotransferase level ratio (alanine transaminase [ALT]/aspartate transaminase [AST]), a measure of liver cell injury, was significantly lower in *Pxdn*^{-/-} mice after 4 weeks of discontinuation of CCl4 compared with the ALT/AST ratio in the *Pxdn*^{+/+} group, which remained high (0.2 ± 0.09 vs 0.7 ± 0.3; $P < .05$) (Figure 9, *C*). As expected, hydroxyproline was elevated in both *Pxdn*^{-/-} and *Pxdn*^{+/+} livers during fibrosis progression and decreased after withdrawal of CCl4, but during regression, *Pxdn*^{-/-} mice showed significant reduction in hydroxyproline measurement compared with *Pxdn*^{+/+} controls (211.6 ± 22.7 vs 352.2 ± 56.9; $P < .05$) (Figure 9, *D*). Collagen staining revealed typical sign of fibrosis remodeling in *Pxdn*^{+/+} controls after 4 weeks of CCl4 withdrawal with widening and splitting of fibrotic septa (Figure 9, *E*). These features were markedly accelerated in *Pxdn*^{-/-} mice. The fibrotic septa were thinner than in *Pxdn*^{+/+} controls, and in some areas, were hardly visible (3.9 ± 1.9 vs 10.5 ± 3.2 μm; $P < .05$) (Figure 9, *F*). Taken together, because of loose collagen structures and more accessibility of poorly crosslinked collagens in *Pxdn*^{-/-} livers, collagen removal occurs faster during fibrosis recovery in *Pxdn*^{-/-} mice.

PXDN Expression Increases With Severity of Fibrosis in Murine Nonalcoholic Fatty Liver Disease

To investigate PXDN in another animal model, we chose a dietary mouse model of nonalcoholic fatty liver disease (NAFLD), known as the choline-deficient, L-amino acid-defined, high-fat diet (CDAHFD). This model recapitulates histological abnormalities similar to those observed in human NAFLD.[42] In the CDAHFD mouse model, the first sign of fibrosis appears by 6 weeks, and mice exhibit hepatic bridging fibrosis by 10 weeks. Continuation of CDAHFD results in cirrhosis and hepatocellular carcinoma (HCC) at 16 weeks. CDAHFD withdrawal results in regression of fibrosis and resolution of scar tissue. In our study, we fed 8-week-old male C57BL/6J mice with CDAHFD for 8, 10, and 16 weeks. In a separate group, CDAHFD was removed after 10 weeks and replaced with normal chow to allow spontaneous recovery of liver for 4 weeks (Figure 10, *A*). Histopathological assessments and collagen staining on liver sections showed severe inflammation, steatosis, and mild fibrosis at 8 weeks, and severe fibrosis along with markedly high inflammation at 10 and 16 weeks in mice fed with CDAHFD (Figure 10, *A*). Gene expression of both *Acta2* and
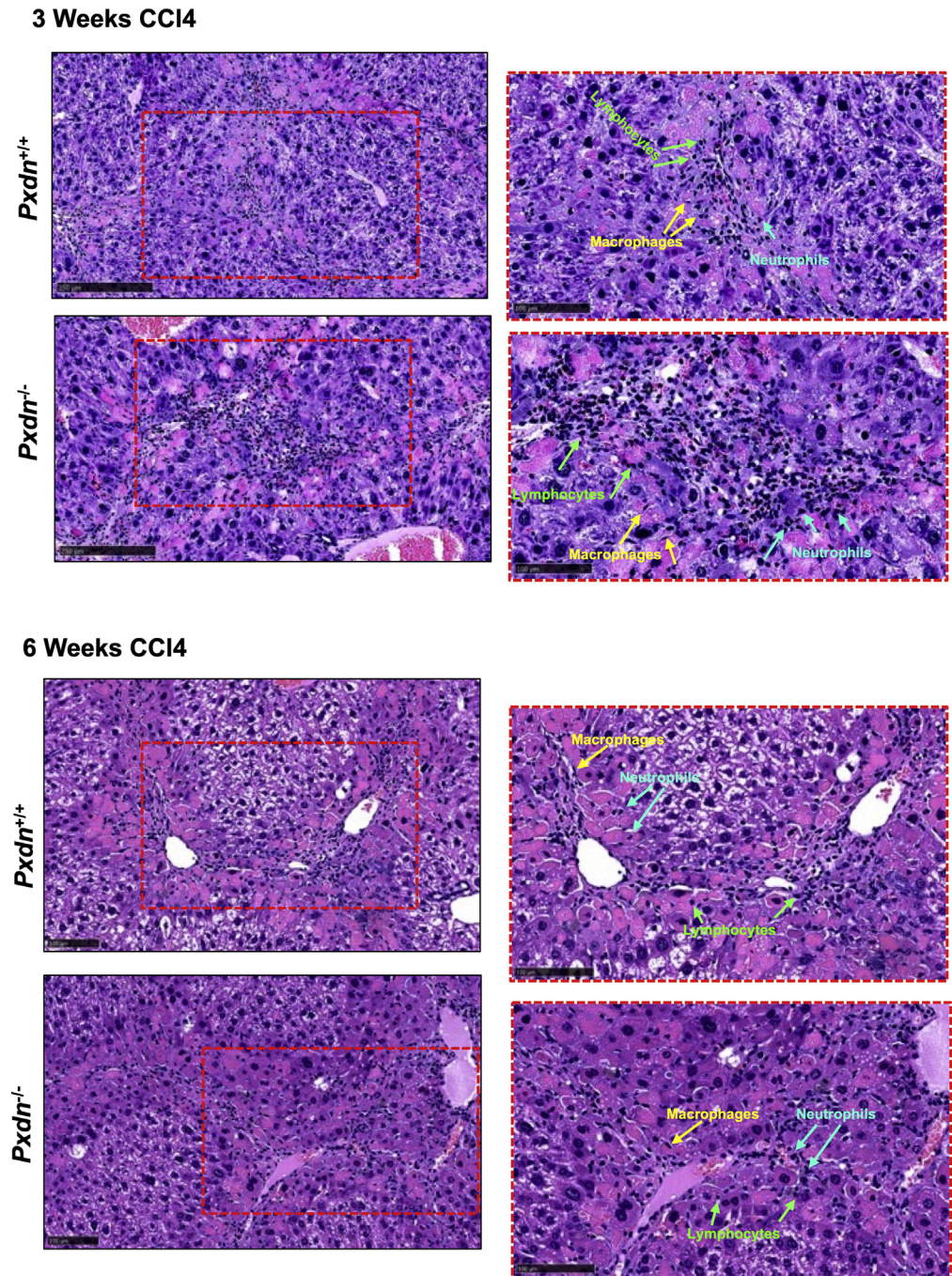
3 Weeks CCl4

6 Weeks CCl4

Figure 5. Increase in immune cell infiltration after liver injury. Histologic examination of liver injury in *Pxdn*^{-/-} and *Pxdn*^{+/+} livers by H&E staining 6 weeks after CCl4 administration shows a significant increase in immune cell infiltration into liver. Representative images from tissue sections with 100-mm scale bar (*left side*) and 50-mm scale bar (*right side*).

Col1a1 increases over time and decreases after removal of CDAHFD (Figure 10, *B*). Interestingly, *Pxdn* mRNA and protein expression shows a similar pattern to *Acta2* and *Col1a1* (Figure 10, *B-C*).

To investigate the role of PXDN in liver fibrosis progression, we fed *Pxdn*^{-/-} and *Pxdn*^{+/+} mice with CDAHFD for 16 weeks. CDAHFD resulted in HCC tumors in wild-type animals, whereas none of the *Pxdn*^{-/-} livers had HCC tumors (Figure 10, *D*). Liver/body weight ratio was not different between *Pxdn* deficient and *Pxdn*^{+/+} animals (Figure 10, *E*); however, spleen/body weight ratio was significantly lower in *Pxdn*^{-/-} mice compared with controls (Figure 10, *F*).

Splenomegaly is defined as enlargement of the spleen measured by weight or size. The increase in the weight/size of the spleen is due to obstruction of blood flow in hepatic or portal veins. In liver cirrhosis, scar tissue can cause the blockage of blood flow through the liver, thus causing blood to back up in the portal vein, resulting in increased pressure or portal hypertension.[43] Histological analysis and quantification of fat deposition showed no difference between *Pxdn*^{+/+} and *Pxdn*^{-/-} mice livers; however, quantification of SR staining for collagen revealed significantly lower collagen proportional area in *Pxdn*^{-/-} livers compared with *Pxdn*^{+/+} mice in mid (8 weeks), and late
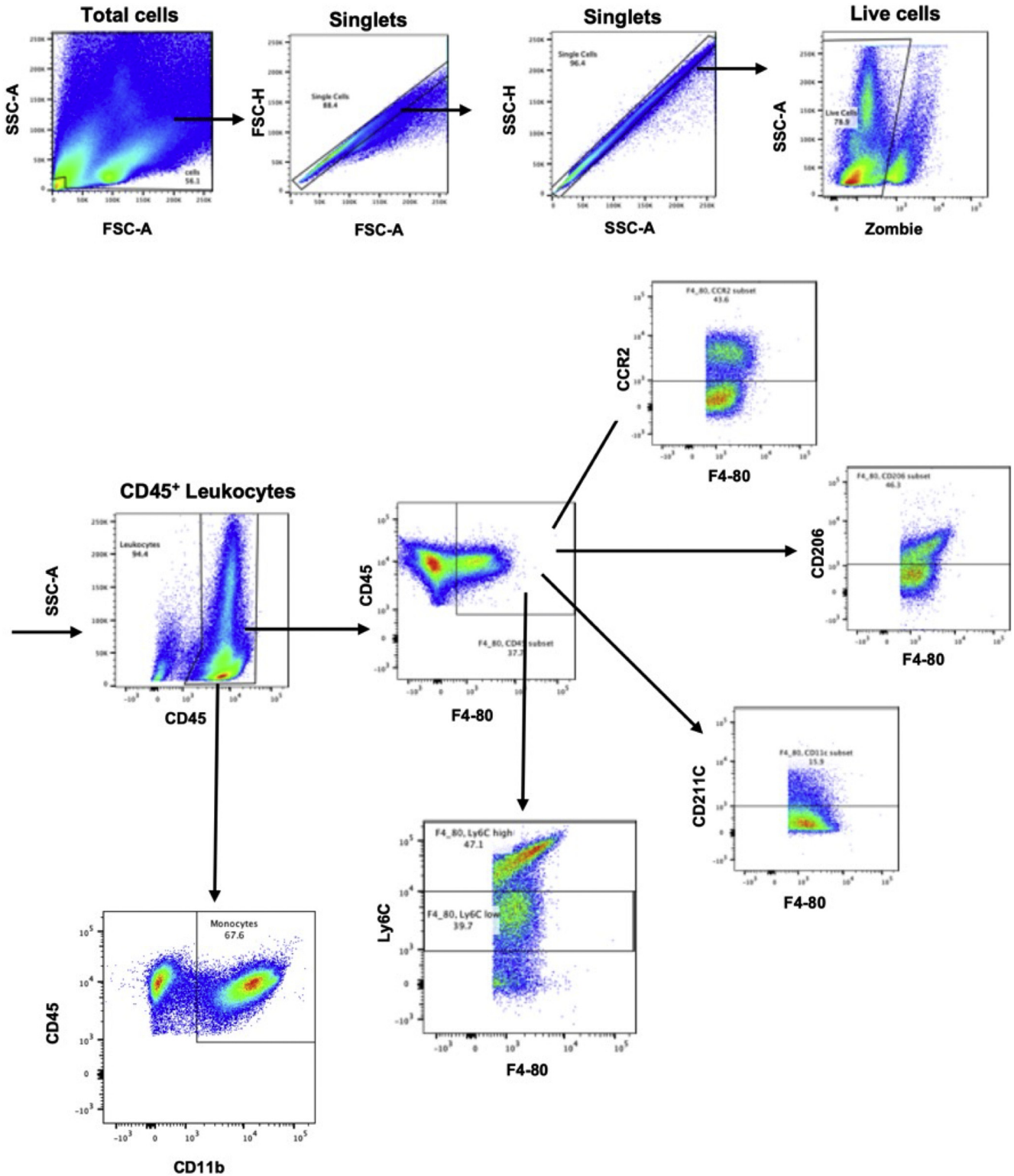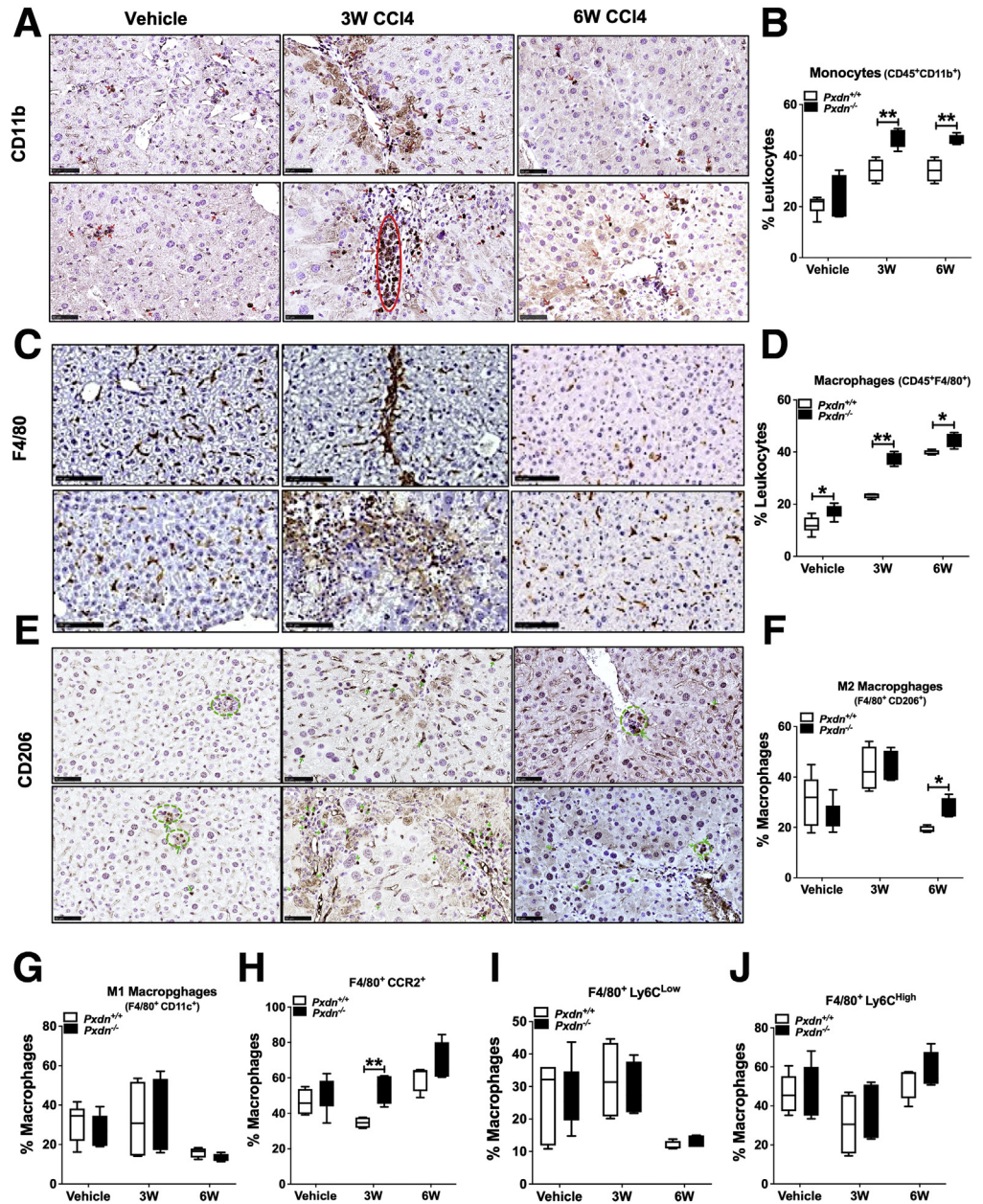
Figure 6. Gating strategy for flow cytometric analysis of liver macrophages. Liver macrophages are identified as CD45⁺F4/80⁺ cells and were gated out of singlet live cells (Zombie⁻ cells). Gated macrophages then analyzed by their expression of CCR2, CD206, CD11c, and Ly6C. In addition, total monocyte population were analyzed based on their CD11b expression. Up to 500K cells were analyzed in each sample.

(16 weeks) stages of NAFLD (Figure 10, *G*). In addition, we observed a reduction in immunohistochemical staining of stellate cell marker ACTA2 in *Pxdn⁻/⁻* mice (Figure 10, *G*). To study the macrophage spatial distribution, we co-stained liver sections collected after 16 weeks of CDAHFD for collagen fibers (SR) and the macrophage
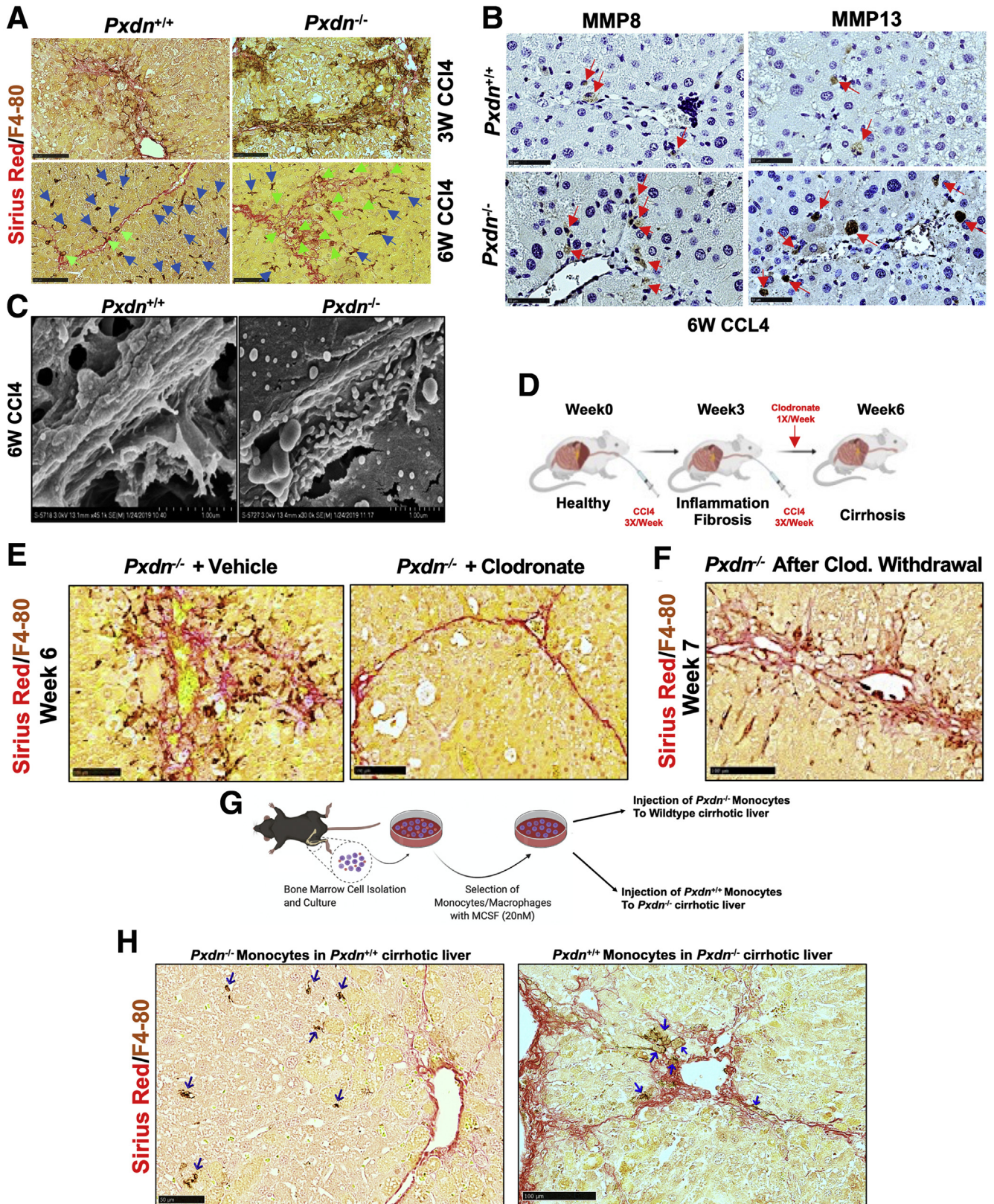
Figure 7. Macrophage characterization in *Pxdn⁻/⁻* livers without and after CCl4 injury. *A*, CD11b immunostaining of liver collected from mice without (vehicle control) or after 3 weeks and 6 weeks of CCl4. *B*, Flowcytometry analysis of monocyte population (CD45⁺CD11b⁺). *C*, F4/80 immunostaining. *D*, Flowcytometry analysis of total macrophage population (CD45⁺F4/80⁺). *E*, Immunohistostaining of CD206 as a marker for pro-resolution macrophages. *F*, Flowcytometry analysis of F4/80⁺CD206⁺ cells (M2 macrophages). Flowcytometry analysis of M1 macrophages (F4/80⁺CD11C⁺) (*G*) and CCR2⁺ migratory macrophages (*H*). *I & J,* Flowcytometry analysis of Ly6C positive macrophages (both low and high expressing) All images have scale bar = 100 mm. (n = 4 mice, mean ± standard deviation, Multiple *t* test, **P < .01).

marker F4/80. We observed that in *Pxdn⁻/⁻* liver, macrophages are in the vicinity of collagen fibers (Figure 10, *H*), a phenotype we previously observed in CCl4-induced liver injury (Figure 8, *A*). We further analyzed the changes in macrophage cell populations during the early (4 weeks), mid (8 weeks), and late (16 weeks) stages of NAFLD by multicolor flow cytometry using the gating strategy and differential expression of cell surface markers described previously (Figure 6). Total population of hepatic macrophages (CD45⁺ F4/80⁺) was significantly increased in *Pxdn⁻/⁻* livers at late-stage fibrosis (23.2 ± 4.5 vs 18.2 ± 4; $P < .05$) compared with their *Pxdn⁺/⁺* littermates (Figure 10, *I*). M1 macrophages (CD45⁺F4/80⁺CD11c⁺) were significantly higher in the early and mid stages of fibrosis in *Pxdn⁻/⁻* livers, whereas M2 macrophages
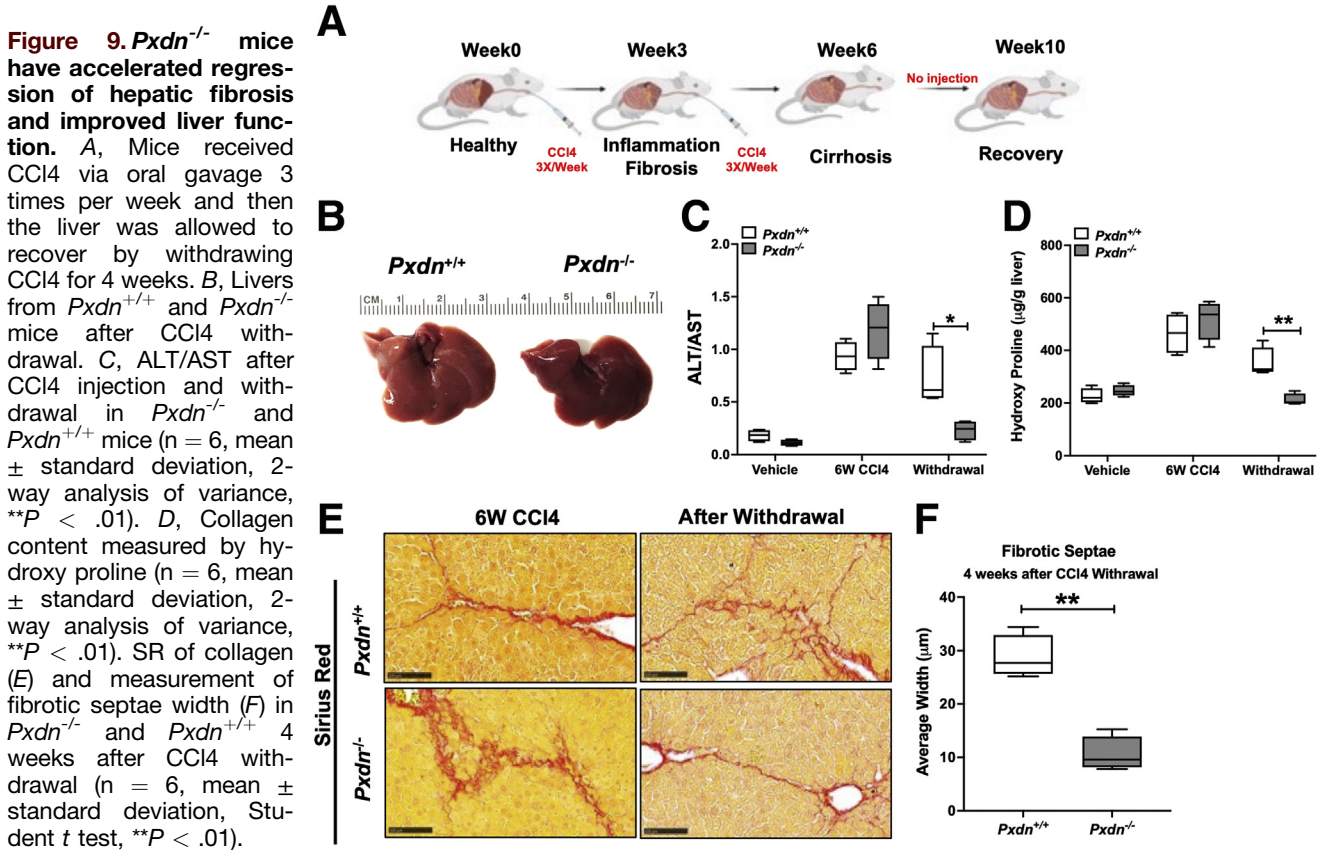
(CD45⁺F4/80⁺CD206⁺) showed significant increase in mid-stage fibrosis.

In *Pxdn⁻/⁻* livers, migratory CCR2⁺ macrophages were significantly higher in mid-stage, whereas they stayed constant at the later time point. Interestingly, recruitment of Ly6C⁺ cells increased in late-stage of fibrosis in *Pxdn⁻/⁻* mice (Figure 10, *I*). Both Ly6C^high and Ly6C^low macrophages were higher in *Pxdn⁻/⁻* livers. Ly6C^high monocytes are initially recruited to the site of injury and then differentiate into Ly6C^low monocytes-derived macrophages.[44] Taken together, consistent with previous data from CCl4-induced liver injury, recruitment of monocytes and macrophages to *Pxdn⁻/⁻* livers is significantly higher during NAFLD, and pro-fibrolysis macrophages are actively involved in the scar tissue resolution from the early stages of fibrosis.

To investigate whether NAFLD regression in *Pxdn⁻/⁻* liver is faster, animals were fed with CDAHFD for 16 weeks and then diet was replaced with normal chow for 2 more weeks.

After the 18 weeks, liver, spleen, and blood were collected for further analysis. Two weeks after diet withdrawal, *Pxdn⁻/⁻* livers showed glossy surface and bright red color,

Figure 9. Pxdn⁻/⁻ mice have accelerated regression of hepatic fibrosis and improved liver function. *A*, Mice received CCl4 via oral gavage 3 times per week and then the liver was allowed to recover by withdrawing CCl4 for 4 weeks. *B*, Livers from *Pxdn*⁺/⁺ and *Pxdn*⁻/⁻ mice after CCl4 withdrawal. *C*, ALT/AST after CCl4 injection and withdrawal in *Pxdn*⁻/⁻ and *Pxdn*⁺/⁺ mice (n = 6, mean ± standard deviation, 2-way analysis of variance, **P < .01). *D*, Collagen content measured by hydroxy proline (n = 6, mean ± standard deviation, 2-way analysis of variance, **P < .01). SR of collagen (*E*) and measurement of fibrotic septae width (*F*) in *Pxdn*⁻/⁻ and *Pxdn*⁺/⁺ 4 weeks after CCl4 withdrawal (n = 6, mean ± standard deviation, Student *t* test, **P < .01).

whereas *Pxdn*⁺/⁺ livers still showed the fibrotic gross phenotype and contained HCC nodules (Figure 11, *A*). Histological analysis showed that fat deposition quickly resolved after CDAHFD removal in both groups; however, *Pxdn*⁻/⁻ livers showed a lower amount of fat compared with their *Pxdn*⁺/⁺ littermates (Figure 11, *B*). Collagen staining with SR showed quicker collagen resolution in *Pxdn*⁻/⁻ livers. In addition, lower ACTA2 staining revealed faster deactivation of stellate cells in *Pxdn*⁻/⁻ mice. Fat content, collagen proportional area, and ACTA2 expression were quantified and showed significant decrease in *Pxdn*⁻/⁻ livers compared with *Pxdn*⁺/⁺ livers after CDAHFD withdrawal (Figure 11, *C*). ALT level was slightly lower in *Pxdn*⁻/⁻ mice as well (Figure 11, *D*). These results confirm that *Pxdn*⁻/⁻ liver has a higher speed of resolution when the insult is withdrawn.

Liver and Serum PXDN Protein Level Increases in Patients With NAFLD

To study the expression pattern of PXDN during NAFLD progression in humans, we stained PXDN in liver biopsy specimens from patients with fibrosis and NAFLD. The stages of NAFLD-associated fibrosis were determined using collagen staining (SR staining) and scored by an expert pathologist. NAFLD specimens were scored based on MET-AVIR system from F0 to F4 as follows: F0, absence of fibrosis; F1, perisinusoidal or periportal fibrosis; F2, combined perisinusoidal and portal/periportal fibrosis; F3, bridging fibrosis; and F4, cirrhosis. In F1 to F4 livers, PXDN expression was detected in fibrotic area and increased with increasing severity of fibrosis (Figure 12, *A*). PXDN was also measured in serum from 92 patients with varying stages of

---

Figure 8. (*See previous page*). Fibrolytic activity of macrophage in *Pxdn*⁻/⁻ livers during fibrosis progression. *A*, Co-staining of macrophages (F4/80 immunohistochemistry) and collagen fibers (SR staining) at 3 weeks and 6 weeks of CCl4 injection in *Pxdn*⁻/⁻ and *Pxdn*⁺/⁺ livers. Macrophages that are directly associated with fibrotic bands are marked green arrows. *B*, IHC of MMP8 and MMP13 in *Pxdn*⁻/⁻ livers after 6 weeks of CCl4 injection. *Green arrows* indicate positive cells for MMP8 and MMP13. *C*, Scanning electron microscope shows an increase in the presence of immune cells next to the fibrotic bands in *Pxdn*⁻/⁻ livers. *D*, Schematic representation of procedure used to deplete liver macrophages with Clodronate-containing liposomes that induce macrophage "suicide program." *E*, Co-staining of macrophages (F4/80 IHC) and collagen fiber (SR staining) shows complete depletion of macrophages in the livers that received clodronate. *F*, Co-staining of macrophages (F4/80 IHC) and collagen fiber (SR staining) 24 hours after chlodronate withdrawal. *G*, Schematic representation of procedure of monocytes transplantation into the mouse liver with opposite genetic background. *H*, Co-staining of macrophages (F4/80 IHC) and collagen fibers (SR staining) 24 hours after transplantation. *Pxdn*⁻/⁻ monocytes that were injected to the wild-type backgrounds are found in the liver parenchyma, whereas the *Pxdn*⁺/⁺ monocytes that were injected to the *Pxdn*⁻/⁻ liver microenvironment are found in the fibrotic tissue (SR positive area). Homing macrophages are shown with *blue arrows*.
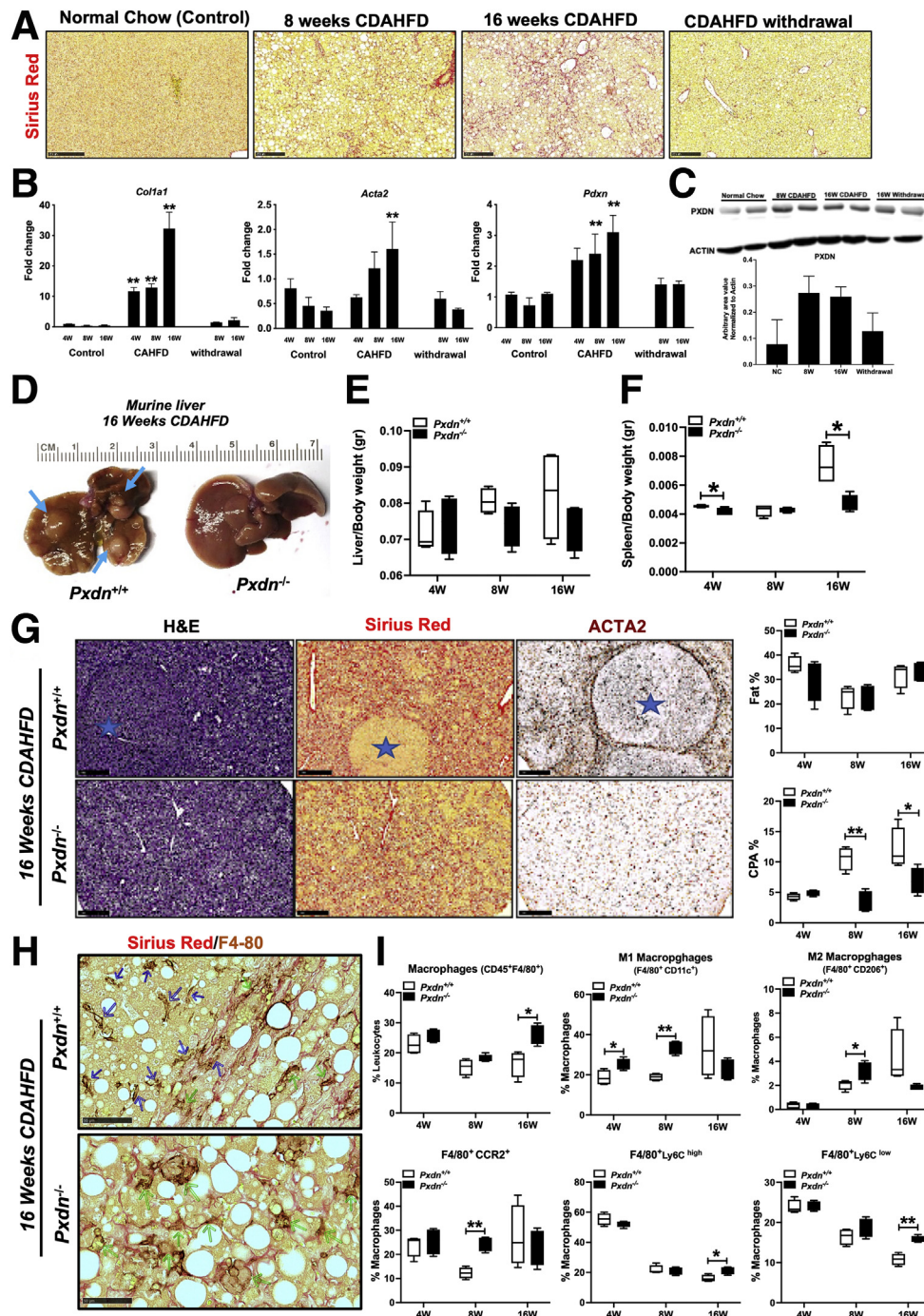
Figure 10. PXDN is upregulated during mouse NAFLD. *A*, SR stained liver sections from mice with or without CDAHFD and after withdrawal of CDAHFD. All images have scale bar = 250 mm. *B*, mRNA expression of collagen (*Col1a1*), *Acta2*, and *Pxdn*. *C*, Western blot analysis of PXDN protein expression in mouse. The graph shows the quantification of PXDN protein expression normalized to ACTIN (n = 2, mean ± standard deviation). *D*, Photos of *Pxdn*^{+/+} and *Pxdn*^{-/-} livers 16 weeks post CDAHFD. *Blue arrows* indicate HCC nodules in *Pxdn*^{+/+} liver. *E & F*, Liver and spleen weights normalized to body weight in early (4 weeks), mid (8 weeks) and late (16 weeks) -stage NAFLD (n = 4, mean ± standard deviation, Multiple *t* test, *$P < .05$ and **$P < .01$). *G*, Livers from *Pxdn*^{+/+} and *Pxdn*^{-/-} mice after 16 weeks of CDAHFD were analyzed by H&E, SR staining, and IHC of ACTA2. *Blue stars* indicate cross-section of HCC nodules. All images have scale bar = 100 mm. (n = 4, mean ± standard deviation, Multiple *t* test, *$P < .05$ and **$P < .01$). *H*, Co-staining of macrophages (F4/80 IHC) and collagen fiber (SR staining) of livers after 16 weeks after CDAHFD in *Pxdn*^{-/-} livers. Macrophages that are directly associated with fibrotic bands are marked with *green arrows*, and macrophages that are outside the fibrotic area are marked with *blue arrows*. Scale bar = 250 mm. *I*, Macrophage characterization in *Pxdn*^{-/-} and *Pxdn*^{+/+} livers during NAFLD progression with flow cytometry (n = 4, mean ± standard deviation, Multiple *t* test, *$P < .05$, **$P < .01$).

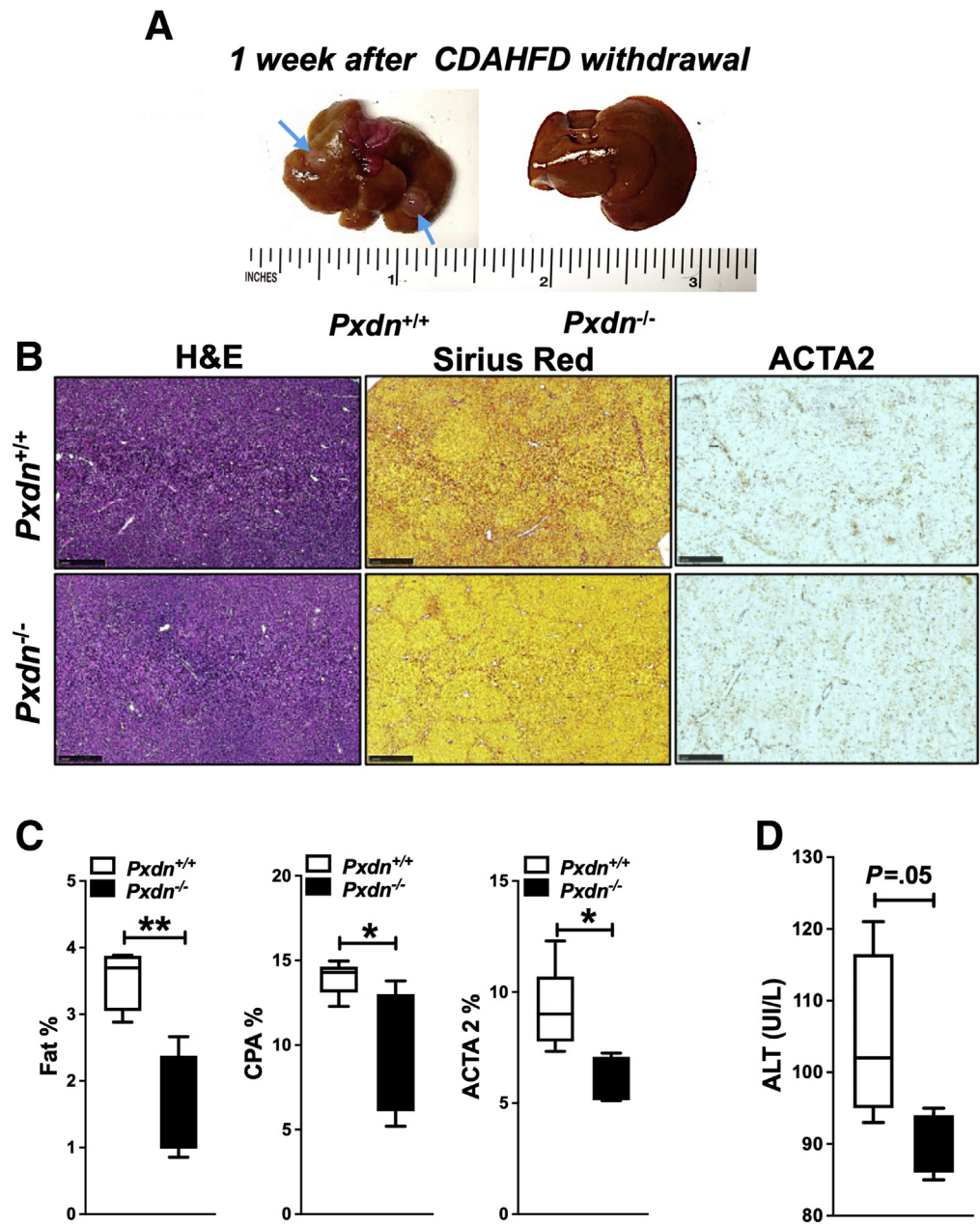**Figure 11.** *Pxdn*^{-/-} mice have accelerated regression of hepatic fibrosis after high fat diet removal. *A*, Photos of *Pxdn*^{+/+} and *Pxdn*^{-/-} livers 2 weeks after CDAHFD withdrawal. *Blue arrows* indicate HCC nodules in *Pxdn*^{+/+} liver. *B & C*, Histological analysis of *Pxdn*^{+/+} and *Pxdn*^{-/-} livers, 2 weeks post CDAHFD withdrawal by H&E, SR staining, and IHC of ACTA2. All images have scale bar =100 mm (n = 4, mean ± standard deviation, Multiple *t* test, $*P < .05$, $**P < .01$). *D*, ALT level decreases slightly faster in *Pxdn*^{-/-} mice.

NAFLD (F0 = 12, F1 = 24, F2 = 17, F3 = 22, F4 = 17) and 10 healthy individuals (Table 2). Serum levels of PXDN were significantly increased in patients with NAFLD compared with healthy individuals. PXDN level increased in patients with all stages of NAFLD compared with the healthy individuals. (Figure 12, *B*). The information about age, gender, and the stage of patients with NAFLD are listed in Table 2.

Activated HSCs Program the Macrophage Recruitment and Function

Among several cell types present in liver, HSCs play a central role in initiation and continuation of immune response to liver injury. Activation of HSCs caused by liver injury is now well-established as a central driver of fibrosis in experimental and human liver injury.[45] Therefore, we aimed to investigate the connection between signals and factors secreted from stellate cells and programming of recruited bone marrow monocytes. We evaluated the ability of monocytes to differentiate into macrophages in vitro after culturing them in conditioned medium collected from activated HSCs.

Primary stellate cells were isolated from healthy liver of *Pxdn*^{+/+} and *Pxdn*^{-/-} mice and activated with TGF-b 24 hours after isolation. Seventy-two hours after HSC activation, the supernatant medium was collected from both conditions, and stellate cells were collected for their gene expression analysis (Figure 13, *A*). As evidenced by quantitative real-time polymerase chain reaction (qPCR) and immunofluorescent staining, TGF-b treatment induced HSC activation
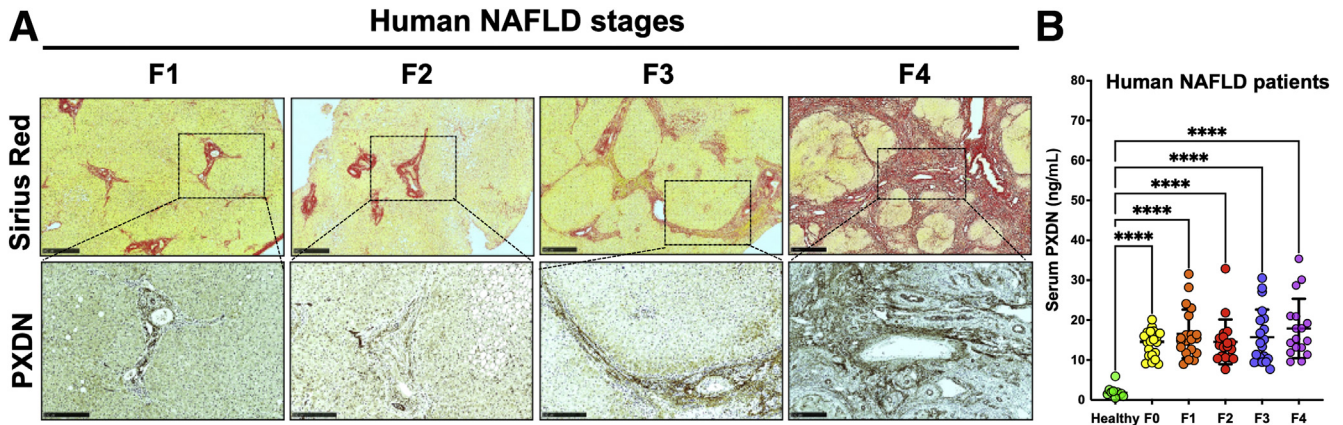
Figure 12. PXDN expression in human NAFLD increases with the severity of the disease in liver tissue and serum. *A*, Collagen staining with SR (Scale bar = 500 mm) and immunohistochemical staining of PXDN (Scale bar = 250 mm) on human liver biopsies. *B*, Serum level of PXDN (ng/mL) in human patients with NAFLD (F0-F4 fibrosis) and healthy controls. (mean ± stand deviation, 1-way analysis of variance, ****$P < .0001$).

with increased expression of smooth muscle actin (*Acta2*) (Figure 13, *B*). mRNA expression analysis revealed upregulation of other markers of activated HSCs, such as *Col1a1, Col3a1, Tgf-b, Ctgf, Lox, IL-6,* and *Ccl2,* and downregulation of *IL-10* after treatment with TGF-b compared with untreated stellate cells from both *Pxdn*^{+/+} and *Pxdn*^{−/−} (Figure 13, *C*). Interleukin (IL)-10 is an anti-inflammatory cytokine that plays a crucial role in preventing inflammatory response to tissue injury. Downregulation of IL-10 increases response to tissue injury and boosts the resolution of associated tissue damage.[46]

To analyze the gene expression of HSCs in vivo, we mapped genome-wide RNA sequencing data collected from CCl4-injured *Pxdn*^{+/+} and *Pxdn*^{−/−} livers to the previously published "Activated stellate cell gene signature" by Zhang et al.[47] Differential gene expression analysis showed that in vivo activated *Pxdn*^{−/−} HSCs upregulate genes involved in ECM production (eg, HS6ST2, GPR176, TGFb3), inflammatory response (eg, LMCD1, LRRN4, TSLP, TGFb3), and cell differentiation (eg, RBM46, FOXS1, ANKRD1 and AHNAK2, KDELR3, FRZB) compared with *Pxdn*^{+/+} controls (Figure 13, *D*). These data suggest important involvement of *Pxdn*^{−/−} HSCs in increased immune cell recruitment and altered matrix remodeling.

We next co-cultured monocytes with conditioned medium from activated HSCs to investigate the migratory and fibrolytic characteristics of differentiated macrophages when exposed to proteins secreted from activated *Pxdn*^{+/+} and *Pxdn*^{−/−} HSCs. We cultured primary monocytes, isolated from tibia and fibula of *Pxdn*^{+/+} adult mice, in the conditioned media collected from *Pxdn*^{+/+} and *Pxdn*^{−/−} activated HSCs for 7 days. One percent FBS and low concentration of M-CSF (20 nM) were supplemented to the conditioned media to support monocyte survival. Mock medium, DMEM supplemented with 1% FBS and M-CSF (20 nM), was used as a control (Figure 14, *A*). After the first 24 hours of in vitro culture, primary monocytes exhibited a round shape with limited spreading on plastic culture plate. After culturing primary monocytes in media conditioned by activated HSCs,

their maturation to macrophages and ability to respond to lipopolysaccharides was measured by gene expression analysis. In comparison with monocytes cultured in conditioned medium from *Pxdn*^{+/+} HSCs, monocytes cultured in conditioned medium from *Pxdn*^{−/−} HSCs had greater mRNA expression of *Cd11b, Ccr2, Ccl2,* and *Il-6* compared with monocytes cultured in conditioned medium from *Pxdn*^{+/+} HSCs and control group.

IL-10 expression was significantly upregulated compared with the control group (Figure 14, *B*). Flow cytometry analysis showed that the expression of liver-specific macrophage marker F4/80 increases significantly in monocytes differentiated to macrophages in conditioned medium from *Pxdn*^{−/−} HSCs compared with the monocytes cultured in *Pxdn*^{+/+} HSCs conditioned medium (91.8 ± 1.9 vs 74.5 ± 4.3; $P < .01$) and control group (91.8 ± 1.9 vs 51.3 ± 14.3; $P < .01$) (Figure 14, *C*).

In addition, CCR2 expression was notably increased on the cell surface of monocytes differentiated in conditioned medium from *Pxdn*^{−/−} HSCs compared with the monocytes cultured in *Pxdn*^{+/+} HSCs conditioned medium (88.4 ± 8.1 vs 52.5 ± 4.5) and control group (88.4 ± 8.1 vs 12.8 ± 7.5; $P < .01$) (Figure 14, *C*). This is consistent with the higher mobility potential of these macrophages in vivo (Figure 7, *H*). Elevated expression of F4/80 in macrophages differentiated in conditioned medium from *Pxdn*^{−/−} HSCs were also assessed by immunocytofluorescent staining (Figure 14, *D*).

Macrophage phagocytic and fibrolytic functions enable wound healing and clearance of fibrotic bands in vivo.[48] Phagocytic capacity of differentiated macrophages was tested by their ability to engulf fluorescein isothiocyanate (FITC)-conjugated Dextran in vitro.[49] We observed that *Pxdn*^{+/+} monocytes that were differentiated to macrophages in conditioned medium from *Pxdn*^{−/−} HSCs exhibited the highest phagocytotic ability compared with monocytes cultured in conditioned medium from *Pxdn*^{+/+} HSCs and control groups (Figure 14, *D-E*). Fibrolytic ability of differentiated macrophages was tested with immunofluorescent staining of MMP8 (collagenase 2). A significant increase in
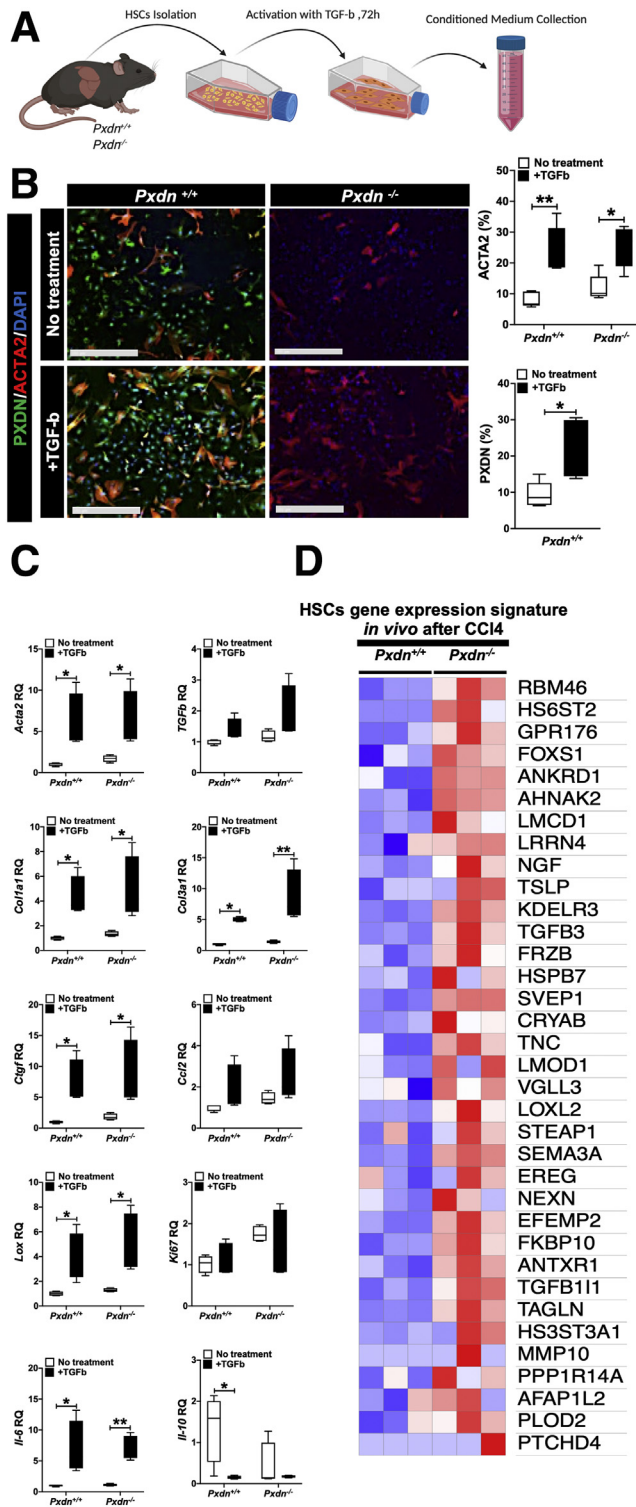
Table 2. Age, Gender, Stage and PXDN Serum Level in Patients With NAFLD

NAFLD stage	F0	F1	F2	F3	F4
Number of values	20	20	18	18	17
Male	3	4	7	6	12
Female	17	16	11	12	6
Mean age, y	51 ± 12	59 ± 12	56 ± 10	66 ± 7	60 ± 10
Minimum	25	33	33	54	43
Maximum	68	76	72	78	73
PXDN level, ng/mL					
Minimum	9	9	8	8	10
Maximum	20	32	33	31	36
Range	11	23	25	23	26
Mean	15	17	15	16	18
Standard deviation	3	6	6	7	7

NAFLD, Nonalcoholic fatty liver disease; *PXDN*, peroxidasin.

MMP8 enzyme was observed in the monocytes that were cultured in *Pxdn*$^{-/-}$ HSCs conditioned medium when compared with monocytes cultured in *Pxdn*$^{+/+}$ HSCs conditioned medium (13 ± 3.1 vs 2.7 ± 1.5; $P < .01$) (Figure 14, *D, F*).

Taken together, these data suggest that *Pxdn*-deficient mice have more resident and infiltrating immune cells to help with the resolution of fibrosis from early stage of fibrosis. Immune cells, particularly macrophages, actively secrete pro-healing MMPs and accelerate the process of tissue restoration. The liver microenvironment, particularly HSCs, plays an important role in programming the recruiting monocyte toward pro-healing and pro-fibrolysis characteristics.

Mechanism Underlying the Activation of Pro-healing Immune Cells in Pxdn-deficient Livers

PXDN belongs to a family of heme-containing peroxidases that catalyze oxidation of various substrates, mainly utilizing the reactive oxygen species (ROS) hydrogen peroxide (H2O2) in the formation of hypohalous acids - HOBr in the case of PXDN.[50]

We previously reported that the redox-active Fe complex Fe-PyC3A serves as a ROS-activated magnetic resonance imaging (MRI) contrast agent that is sensitive to changes in redox state of the tissue microenvironment and inflammation in vivo.[51] In the 2+ oxidation state, Fe^{2+}-PyC3A has very low relaxivity and produces negligible MRI signal change when administered to an animal. However, in the presence of ROS, Fe^{2+}-PyC3A is instantaneously converted to Fe^{3+}-PyC3A, which has an order of magnitude higher relaxivity than the 2+ form and is readily detectable by MRI. We used this contrast-enhanced MRI technique to compare

Figure 13. Activated HSCs isolated from *Pxdn*$^{-/-}$ livers have a different mRNA expression profile. *A*, HSCs were isolated from *Pxdn*$^{+/+}$ and *Pxdn*$^{-/-}$ livers and treated with TGF-b for 72 hours to activate HSCs. After 72 hours, conditioned medium was collected, and HSCs were obtained for RNA and protein analysis. *B*, Immunofluorescent staining of PXDN and ACTA2 in HSCs before and after activation with TGF-b. Scale bar = 250 mm. *C*, mRNA expression analysis of quiescent and activated HSCs in vitro shows a significant increase in the expression of critical genes after activation (n = 4, mean ±

standard deviation, Multiple *t* test, *$P < .05$ and **$P < .01$). *D*, Genome-wide gene expression analysis of HSCs gene signature in activated HSCs isolated from *Pxdn*$^{+/+}$ and *Pxdn*$^{-/-}$ livers 6 weeks post CCl4 administration shows differentially expressed genes in *Pxdn*$^{-/-}$ HSCs.
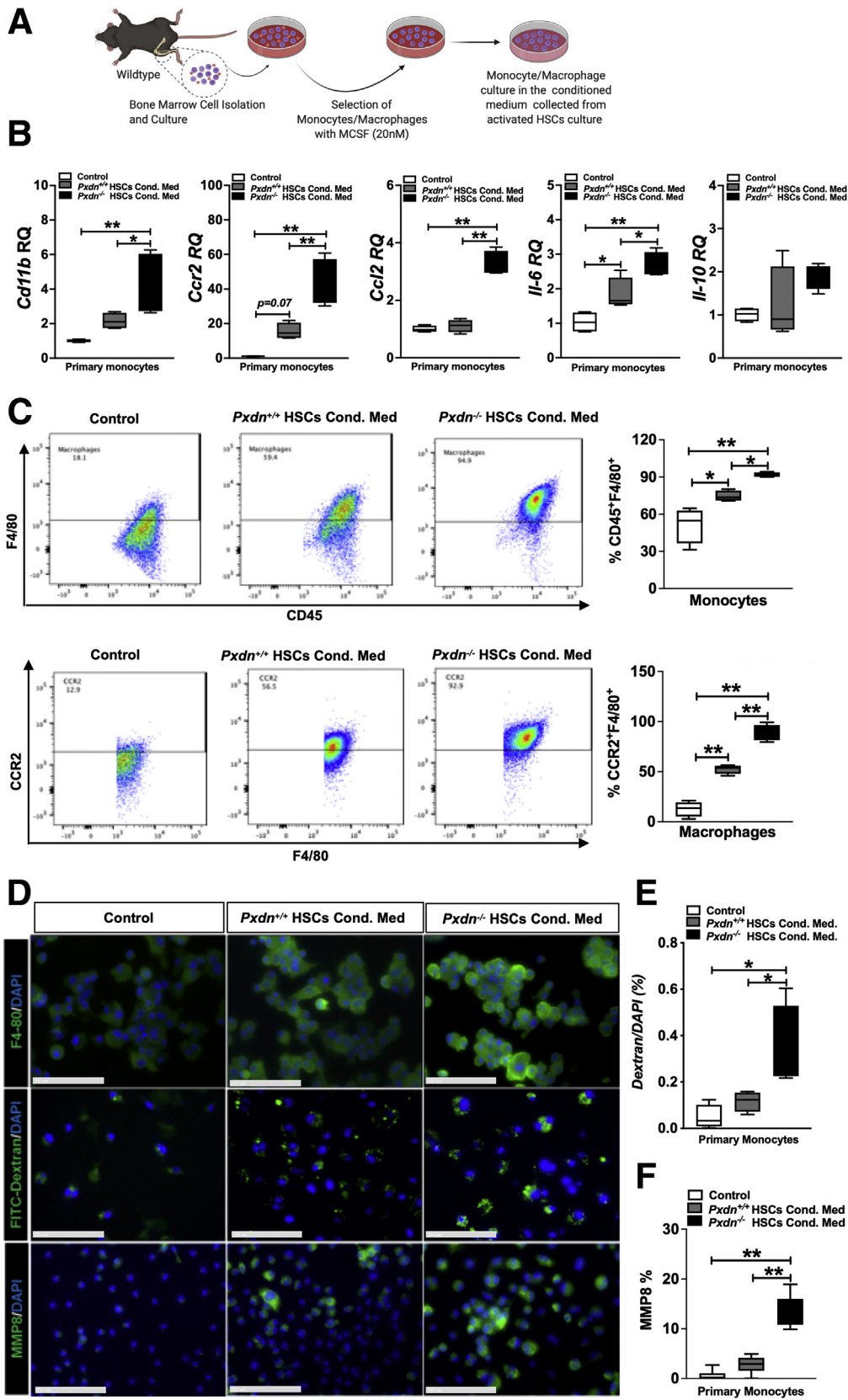
Figure 14. Co-culture of primary monocytes with Pxdn$^{-/-}$ HSCs in vitro can program monocyte differentiation into macrophages. *A*, Schematic overview of monocyte isolation and culture in Pxdn$^{+/+}$ and Pxdn$^{-/-}$ HSCs conditioned medium. *B*, mRNA expression analysis of *Cd11b, Ccr2, Ccl2, Il-6*, and *Il-10* of primary monocytes cultured in Pxdn$^{+/+}$ and Pxdn$^{-/-}$ HSCs conditioned medium. Control monocytes were cultured in basic DMEM supplemented with MCSF (20 nM). *C*, Flow cytometry analysis F4/80 and CCR2 expression on monocytes cultured in Pxdn$^{+/+}$ and Pxdn$^{-/-}$ HSCs conditioned medium. *D*, Immunofluorescent staining of F4/80 in monocyte cultured in Pxdn$^{+/+}$ and Pxdn$^{-/-}$ HSCs conditioned medium. Scale bar = 250 mm. *D & E*, Phagocytosis capacity of macrophages was evaluated by their ability to engulf complex branched carbohydrates such as Dextran conjugated to FITC. Scale bar = 250 mm. *D & F*, Fibrolysis capacity of differentiated macrophages from monocytes cocultured with HSCs, was evaluated by their expression of matrix degrading enzyme, MMP8 (n = 4, mean ± standard deviation, 1-way analysis of variance, *P < .05 and **P < .01).

the ROS level in healthy $Pxdn^{+/+}$ vs. $Pxdn^{-/-}$ livers. T1-weighted MR images were acquired in healthy $Pxdn^{+/+}$ and $Pxdn^{-/-}$ mice before and immediately after intravenous injection of Fe^{2+}-PyC3A. Figure 15, A shows axial images before (left) and after (middle) Fe^{2+}-PyC3A administration. In the $Pxdn^{+/+}$ mice, the MRI liver signal is unchanged after contrast agent injection, whereas in $Pxdn^{-/-}$ mice there is a clear increase in liver signal after Fe^{2+}-PyC3A injection. The right panel is a color overlay that quantifies this change in liver-to-muscle contrast to noise ratio (DCNR) after contrast agent administration on a pixel-wise basis. Figure 15, B shows that DCNR is significantly higher in $Pxdn^{-/-}$ livers compared with $Pxdn^{+/+}$ livers and indicate that there is more ROS in healthy $Pxdn^{-/-}$ livers.

To further investigate whether $Pxdn^{-/-}$ livers differ from $Pxdn^{+/+}$ livers in response to injury, we looked at differentially expressed genes in $Pxdn^{+/+}$ and $Pxdn^{-/-}$ CCl4-injured (after 6 weeks of CCl4 administration) and uninjured livers. Once the overexpressed genes were established, a Gene Ontology (GO) Enrichment Analysis was performed to find the pathways enriched in $Pxdn^{-/-}$ vs. $Pxdn^{+/+}$ mice. GO Enrichment Analysis revealed that the expression of genes involved in hypoxia and TNFA_SIGNALING_VIA_NFKB pathways were up-regulated in $Pxdn^{-/-}$ uninjured livers compared with uninjured $Pxdn^{+/+}$ livers (Figure 15, C). In CCl4-injured livers, EMT and allograft rejection pathways were upregulated pathways in $Pxdn^{-/-}$ injured livers compared with $Pxdn^{+/+}$ injured livers (Figure 15, C). Analysis of RNA-sequencing data indicated that, in uninjured livers, the expression of many genes was strongly increased in $Pxdn^{-/-}$ livers compared with uninjured $Pxdn^{+/+}$ livers. Specifically, 4 major gene programs were activated: Hypoxia (FOS, TNF-a, NF-kB, JUN, DDIT4, DUSP1, ADM, NFIL3, IRS2, KLF6, CDKN1A, IGFBP-1), HSC activation (lysyl oxidase [LOX], MYC, ACTA2, LOXL1, tissue inhibitors of metalloproteinases [TIMP]1, PDGFRB), Cytokine signaling (IL-23, IL1B, CD86, CCRL2), and ECM remodeling (ITGA2, COL5A3, FBN1, ECM2) (Figure 15, D). After 6 weeks of CCl4 administration, 3 major gene programs were up-regulated in $Pxdn^{-/-}$ livers: HSC activation (FBN2, COMP, TIMP1, LOX, ACTA2, LOXL1, LOXL2, WNT5A, EMP3, TGF-b), Cytokine signaling (IL-6, IL2RG, IL-15, CXCR3, CXCL6, CCL5, IL-12A, IL10, IL-7, CD86, CCL2, IL-16, CD80, TLR-1, IL-11, CCL13, CCR2, CD4, IL-15, CCR5, IL-1B), and ECM remodeling (FBN2, COL8A2, MMP3, COL11A1, MMP2, COL1A1, ECM2, MMP9) (Figure 15, E).

Together, GO analysis identified significant upregulation of genes in hypoxia and TNF-a signaling pathways already existing in $Pxdn^{-/-}$ healthy livers. Six weeks after CCl4 injury, upregulation of genes involved in the innate immune response, leukocyte activation, and chemotaxis was observed (Figure 15, E). We speculate that in the absence of PXDN, even without injury, liver tissue redox state changes and results in the activation of hypoxia related genes. This can directly activate TNF-a signaling pathways in the liver and, as a result, increase the recruitment of immune cells such as macrophages and monocytes in the early stage of liver fibrosis (Figure 15, F).

Discussion

The balance between ECM deposition and degradation influences the speed of liver fibrosis progression and regression.[1] Liver fibrosis results from a chronic response to persistent injuries, and is characterized by hepatocyte death, recruitment of immune cells, and activation of ECM-producing stellate cells. Regression of fibrosis is characterized by digestion of ECM, apoptosis of ECM-secreting cells, hepatocyte regeneration, and consequent improvement in organ function. Although the mechanisms that promote collagen synthesis and deposition by stellate cells have been extensively studied, the mechanisms regulating collagen degradation and resolution of fibrosis have been less well-characterized. Strategies to promote resolution of fibrosis include the induction of apoptosis by myofibroblasts, inhibition of collagen cross-linking, and triggering degrading and clearance of ECM.[52] In this study, we identified a hepatic microenvironment with moderately elevated levels of ROS, in which hepatic macrophages digest collagen fibers and inhibit formation of dense fibrotic tissue in the early stages of liver fibrosis. Here, the elevation of ROS levels is associated with deficiency of PXDN, a highly conserved member of the heme-containing peroxidase family, which catalyzes the oxidation of various substrates in the presence of H2O2 and plays a vital role in the inhibition of ROS formation and oxidative stress.[17] Oxidative stress can significantly impact redox-sensitive molecules and act as a second messenger to trigger intracellular signaling pathways.[53] In addition, PXDN contributes to basement membrane assembly via its role in creating sulfilimine bonds in the Col IV network during ECM formation and in ECM-mediated signaling and cell growth pathways.[54,55]

In this study, we showed that in human cirrhotic livers, PXDN is upregulated in stellate cells (ACTA2-expressing cells) and in fibrotic bands. In vitro studies showed that activated HSCs produce and secrete PXDN into the fibrotic microenvironment. In addition, serum levels of PXDN increase significantly in patients with end-stage liver fibrosis. Secretion of PXDN from myofibroblasts occurs in other organs such as heart and kidney and is TGF-b dependent.[18,56] Elevation of PXDN in serum has been reported in patients with peripheral artery disease and is tightly associated with kidney function of patients with peripheral artery disease.[57] PXDN is a very conserved protein among the animal kingdom, and its expression is tightly regulated.[58] It is considered as an ECM-associated molecule, and in mice, unlike abundant proteins in fibrotic tissues like collagen, $Pxdn$ had a moderate upregulation during liver fibrosis.

Mutation causing PXDN loss of function in both human and mice results in congenital cataract-microcornea with corneal opacity, glaucoma, buphthalmos, and extensive corneal opacification.[20,21] We did not detect abnormal liver histology or function in $Pxdn^{-/-}$ mice; however, $Pxdn$ deficiency in the model of CCl4-induced liver injury resulted in abnormal fibrotic septae formation. The divergent phenotype of fibrotic bands in $Pxdn^{-/-}$ mice compared with $Pxdn^{+/+}$ mice started from 3 weeks of CCl4 injection and continued to progress further until the late stage of fibrosis.

Initially, we examined the possibility of PXDN activity in collagen IV cross-linking in liver fibrosis, but surprisingly, collagen IV monomer numbers did not change in the $Pxdn^{-/-}$ fibrotic liver compared with $Pxdn^{-/-}$ healthy controls.

Collagen IV is found in the perisinusoidal basement membrane, and its content increased 16-fold in cirrhotic liver, but progression of F1 to F3–F4 stages of liver fibrosis requires a progressive accumulation of fibrillar collagens
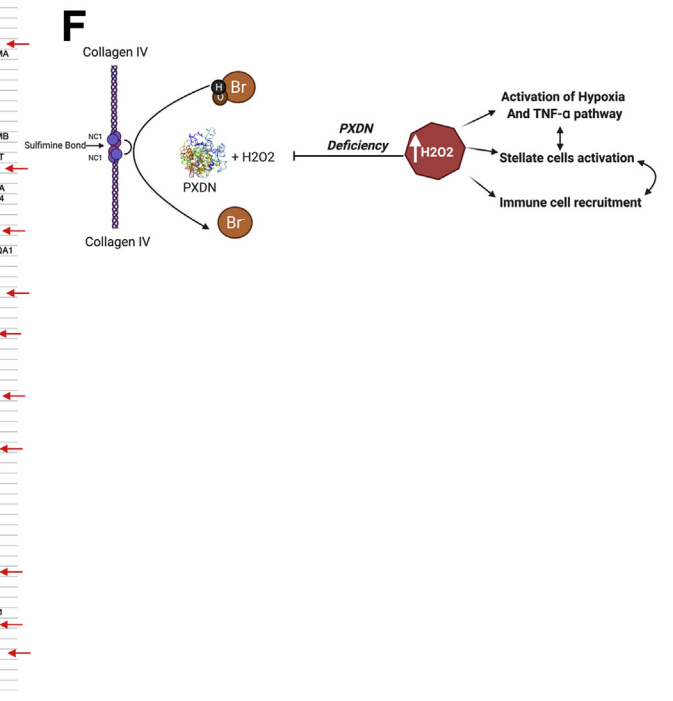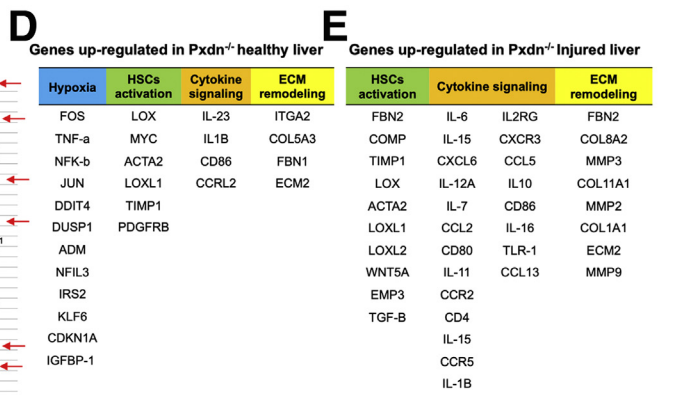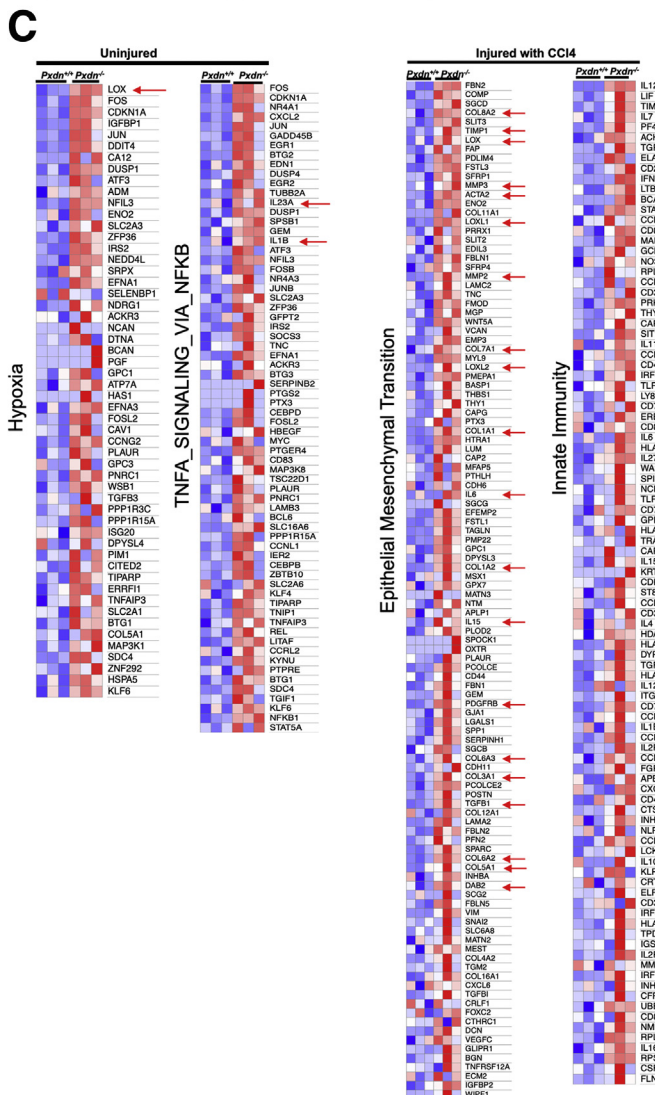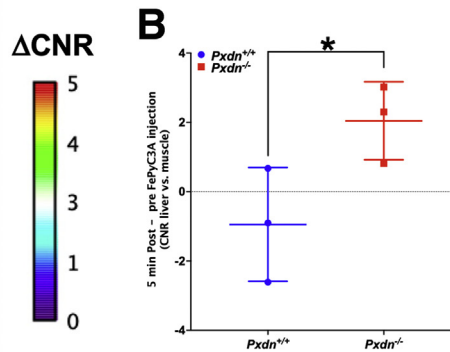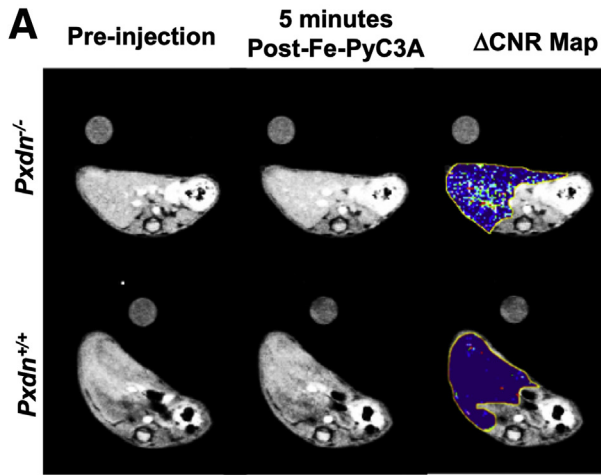
(type I and III).[59] Our observation is similar to previous studies in which lysyl oxidase (LOX) enzyme was experimentally inhibited by b-aminopropionitrile.[28] As a result, the accumulation of cross-linked collagen was decreased, and fibrotic septa showed widening comparable to changes observed during fibrosis resolution in the current study.[28] Due to the chicken-wire phenotype of fibrosis produced in the CDAHFD model, loose formation of collagen bundles was difficult to see in the CDAHFD model of nonalcoholic steatohepatitis in $Pxdn^{-/-}$ liver. Nevertheless, we were able to see the presence of macrophages in the fibrotic tissue at the cirrhosis stage in $Pxdn^{-/-}$ livers. In both liver injury models in $Pxdn^{-/-}$ mice, we observed greater infiltration of macrophages into the liver.

Total hepatic macrophages, consisting of liver resident Kupffer cells and monocyte-derived macrophages, contribute to maintaining homeostasis of the liver as well as the progression of acute or chronic liver injury. During fibrosis, Kupffer cells recruit monocytes and other inflammatory cells and activate stellate cells to produce ECM. On the other hand, macrophages also release MMPs, which promote fibrotic ECM degradation, and factors that dampen the inflammatory response and promote resolution of fibrosis and liver regeneration. We aimed to examine total macrophage populations in 2 different stages of CCl4-induced liver fibrosis: (1) peak of inflammation and early stage of fibrosis (3 weeks of CCl4 injection), and (2) advanced fibrosis (6 weeks of CCl4 injection). We also examined total macrophage populations in 3 stages of NAFLD: early (4 weeks), mid (8 weeks), and late (16 weeks) post CDAHFD.

In general, total macrophage populations boost during the peak of inflammation due to an increase in their proliferation and recruitment of monocytes from bone marrow.[7,60,61] In our animal models, we detected an increase in the number of macrophages ($CD45^+F4/80^+$) in $Pxdn^{-/-}$ livers at the peak of inflammation and late stage liver fibrosis compared with the $Pxdn^{+/+}$ controls. Moreover, macrophages in $Pxdn^{-/-}$ fibrotic livers demonstrated a different phenotype in which they were found inside the fibrotic bands and in close proximity to collagen fibers. As the disease continues, this close proximity became more evident, with concomitant disorganized and loosely connected fibrotic tissue. This phenotype has been reported during the resolution or regression phase in liver injury animal models[28,62] and in human cirrhotic patients. Notably,

we detected it from early stage CCl4-induced fibrosis in $Pxdn^{-/-}$ livers. Detailed characterization of this unique macrophage population found in $Pxdn^{-/-}$ livers revealed that they express higher levels of CD206 (Mannose Receptor) at the late stages of fibrosis and have higher phagocytosis and fibrolytic capacities. $CD206^+$ macrophages are the major source of matrix degrading enzymes, MMPs, and their involvement during fibrosis can interrupt the formation of fibrotic band and progression of fibrosis to irreversible cirrhosis.

Contribution of monocytes ($CD45^+CD11b^+$) is another important factor to consider, where we found notable increase in the number of monocytes in $Pxdn^{-/-}$ livers in the peak of inflammation. In addition, we detected a significant increase in the number of CCR2-expressing macrophages in $Pxdn^{-/-}$ livers during fibrosis progression in both animal models. However, we observed increase infiltration of circulating $Ly6C^+$ monocytes only in the NAFLD animal model. The impact of $Ly6C^+$ monocytes in the induction and resolution of liver fibrosis has been evaluated with conflicting results, and their function can vary between different animal models.[63]

Liver tissue microenvironment, including soluble mediators and cytokines secreted by activated HSCs and other immune cells, can influence the phenotypes of macrophages, and determine their involvement in deterioration of liver injury or restoration of liver functions.[64,65] HSCs play a major role in orchestrating the inflammatory response to injury. In humans, activated HSCs induced infiltration of migratory macrophages ($CD163^+$) via the CCL2/CCR2 pathway.[66] CCL2 is chemokine for CCR2 migratory monocytes, and CCR2 and/or CCR5 antagonism has led to decreased inflammatory monocytes in the liver in a variety of disease models.[67] In our study, we investigated the possibility of stellate cell-initiated pathways of recruitment and maturation of macrophages by in vitro co-culture of bone marrow-derived primary monocytes and $Pxdn^{-/-}$ stellate cells. In this experiment, we found greater expression of CD11b and CCR2 markers in matured macrophages co-cultured with $Pxdn^{-/-}$ stellate cells. In addition, in vitro data confirmed the higher phagocytic activity of macrophages co-cultured with $Pxdn^{-/-}$ stellate cells.

To investigate the underlying mechanism of higher macrophage recruitment in $Pxdn^{-/-}$ liver, we studied the effect of $Pxdn$ deficiency on the redox state of liver tissue as the formation and accumulation of ROS can affect

---

Figure 15. (*See previous page*). **Hypoxic condition caused by *Pxdn* deficiency results in increase of immune cell recruitment during liver injury.** *A*, Representative axial MR images showing the livers of healthy $Pxdn^{+/+}$ and $Pxdn^{-/-}$ before (*left*) and 5 minutes after (*middle*) injection of ROS-specific MRI contrast agent Fe^{2+}-PyC3A, and the pixelwise change (*middle image – left image*) in liver-to-muscle contrast to noise ratio DCNR overlaid (*right image*) shows a strong increase in liver MRI signal in the $Pxdn^{-/-}$ mice but not in the $Pxdn^{+/+}$ animals. *B*, Quantification of MRI data shows significantly higher DCNR (n = 3, mean ± standard deviation, Student t test, *$P < .05$) in $Pxdn^{-/-}$ animals compared with $Pxdn^{+/+}$ mice. *C*, Genome-wide expression analysis, heat maps showed gene expression changes in $Pxdn^{+/+}$ and $Pxdn^{-/-}$ vehicle controls (without injury) and CCl4 (injured) livers (n = 3). *Red arrows* indicate cytokines that attract immune cells to the site of injury. *Red and blue colors* in the heat map indicate up- and down-regulation of gene expression, respectively. *D & E*, Top up-regulated genes in $Pxdn^{-/-}$ livers (healthy and injured) are categorized into 4 different categories: hypoxia, HSCs activation, cytokine signaling, and ECM remodeling. *F*, Schematic representation of the proposed mechanism of $Pxdn$ deficiency on liver fibrosis. $Pxdn$ deficiency results in accumulation of H2O2 of which subsequently contributes to activation of hypoxia and TNF-a pathway, stellate cell activation, and immune cell recruitment to the liver.

polarization of macrophages.[15] PXDN is an oxidase enzyme that uses $H2O2$ to form sulfilimine bonds and cross-link collagen IV.[68] Using redox-active iron complex Fe-PyC3A as an MRI contrast agent, we detected higher content of ROS in $Pxdn^{-/-}$ livers. This high content was not necessary toxic but was associated with upregulation of hypoxia-related molecular pathways and increased expression of ECM regulatory proteins and immunomodulatory cytokines in healthy and injured $Pxdn^{-/-}$ livers. The activation of redox-sensitive transcription factors, such as NF-κB, is necessary for the induction of inflammatory gene expression and recruitment of immune cells. Genome-wide expression analysis showed that the TNF-a pathway via the NF-kB pathway is upregulated in $Pxdn^{-/-}$ livers. This supports the hypothesis that the liver microenvironment plays an important role in programming recruited monocytes and macrophages.

In conclusion, our findings provide new evidence that recruited monocytes from bone marrow are programmed by the liver microenvironment during liver injury. We report a novel microenvironment where macrophages undergo maturation faster and acquire pro-resolution characteristics from the early stages of liver fibrosis. Our data will help further understanding of hepatic immune homeostasis and has implications for the development of novel immunotherapeutic strategies for chronic liver diseases.

Methods
Animals

All animal experiments were approved by the Massachusetts General Hospital Institutional Animal Care and Use Committee (IACUC). Animals were maintained on a 12-hour light/dark cycle at 25 °C and fed a standard diet. C57BL/6J mice were purchased from Charles River Laboratories (Wilmington, MA). $Pxdn^{-/-}$ mice were kindly provided by Dr Gautam Bhave from Vanderbilt University Medical Center (Nashville, TN). To induce liver injury by toxin and cause fibrosis and cirrhosis, mice were given 3 times per week of 20% to 40% CCl4 via oral gavage (Sigma-Aldrich, St. Louis, MO) according to our established protocols.[69] To create NAFLD animal model, 8-week-old male C57BL/6J mice were purchased from Charles River Laboratories (Wilmington, MA) and housed in a specific pathogen-free environment according to our IACUC protocol. After 1 week of acclimation, mice were fed on either normal chow (Prolab Isopro 3000; Scotts Distributing #8670) or L-amino acid diet with 60 kcal% fat with 0.1% methionine without added choline (CDAHFD; Research Diets A06071302) for 16 weeks. In both models, the well-being of animals was observed daily, and with any sign of distress or pain, mice were euthanized immediately.

RNA Extraction and qPCR

RNA was isolated from liver tissue using TRIzol (Life Technologies, Grand Island, NY) according to the manufacturer's instructions and then treated with DNAse I (Promega, Madison, WI). Total RNA (1 μg) from each sample was used to synthesize complementary DNA by single-strand reverse transcription (SuperScript III First-Strand Synthesis SuperMix; Life Technologies). Primer and probe sequences for qPCR were purchased from Applied Biosystems Inc.

Genome-wide Gene Expression Profiling and Data Analysis

Total RNA was isolated as described above. Genome-wide gene expression profiling was performed using high-throughput Illumina HiSeq sequencing in High-Output mode with Single-end 75-bp 20 million reads per sample (Illumina, San Diego, CA). Scanned data were normalized using a cubic spline algorithm, summarized into official gene symbol, and mapped to human orthologous genes using the mapping table provided by the Jackson laboratory (www.informatics.jax.org). Genes were rank-ordered according to differential expression between the experimental conditions. Over- or under-representation of each gene signature on the rank-ordered gene list was evaluated based on random permutation test. False discovery rate <0.25 was regarded as statistically significant. All data analysis was performed using GenePattern analysis toolkit (www.genepattern.org) and R statistical computing language (www.rproject.org).

Single-cell Suspension and Flow Cytometry

Mice were anesthetized using 100 mg/kg of ketamine and 10 mg/kg of xylazine intraperitoneally, followed by terminal cardiac puncture. Animals received humane care per criteria outlined in the Guide for the Care and Use of Laboratory Animals by the National Academy of Sciences (National Institutes of Health publication 86-23, revised 1985) and in accordance with the Massachusetts General Hospital IACUC guidelines. The entire left lobe of liver was cut into small pieces and further digested with collagenase type XI (0.25 mg/ml in Hanks' Balanced Salt Solution [HBSS], Sigma) and deoxyribonuclease 1 (20 units/ml, Roche Diagnostics) at 37 °C for 25 to 35 minutes with gentle agitation, followed by collagenase neutralization with cold phosphate-buffered saline (PBS) containing 10% FBS (Gibco-Invitrogen). Digested tissue was then centrifuged at 50g for 3 minutes to pellet hepatocytes. The supernatant containing the nonparenchymal cells was harvested and filtered through a 70-μm cell strainer to remove cell debris. Purified cells were suspended in 4 mL of 80% isotonic Percoll, and 1 layer of 40% Percoll was added on the top, followed by centrifugation at 3000 RPM for 30 minutes at room temperature with minimum break speed. The cells were aspirated from the Percoll interface and harvested by centrifugation and washed twice with PBS containing 10% FBS. Isolated cells were incubated in FC block (anti-mouse CD16/32) (1:1000, BioLegend) for 10 minutes. Next, cells were stained with fluorochrome conjugated antibodies listed in Table 3 for 30 minutes followed by 3× wash in PBS containing 10% FBS. Then cells were stained with Zombie Aqua Fixable Viability for 10 minutes. After wash with PBS, cells were fixed in paraformaldehyde 2% and run on the LSRII flow cytometer (BD Biosciences, San Jose, CA). Data

Table 3. Antibody Panels for Flow Cytometric Analysis of Liver Monocyte and Macrophages

Conjugated antibody	Clone	Cat#
Alexa Fluor 488 anti-mouse CD11c	N418	117311
PE/Cy7 anti-mouse CD206 (MMR)	C068C2	141719
APC anti-mouse Ly-6C	HK1.4	128015
Brilliant Violet 650 anti-mouse/human CD11b	M1/70	101239
PerCP/Cyanine5.5 anti-mouse CD45	30-F11	103132
Alexa Fluor 700 anti-mouse F4/80	BM8	123129
Brilliant Violet 785 anti-mouse CD192 (CCR2)	SA203G11	150621

were acquired using BD FACSDIVA software (BD Biosciences). The gating strategies are described in Figure 6. FACS data were analyzed using FlowJo, version 10.1 (Ashland, OR).

Tissue Processing and Immunostaining

Formalin-fixed paraffin-embedded tissues samples were sectioned with 5-μm thicknesses and stained with H&E, SR, and immunostaining for alpha-smooth muscle actin (α-SMA, ACTA2) (1:100, Sigma-Aldrich St. Louis, MO) and collagen, Type 1, alpha 1 (COL1A1) (1:200, Abcam, Cambridge, UK), Pxdn (provided by Dr Gutam, 1:200), and CD11b (1:100, Novus Biologicals, Centennial, CO), CD206 (1:100, Novus Biologicals) according to standard protocols, as reported previously.[70] For tissue analysis using the SEM, formalin-fixed and paraffin-embedded sections were incubated in osmium tetroxide (0.5%; Electron Microscopy Sciences, 19152) before serial dehydration in ethanol. Samples were then dried using a critical point drier and imaged using field emission SEM (Hitachi S-4700).

Image Acquisition and Analysis

Fluorescent images were captured with a Nikon Eclipse microscope equipped with an Insight CMOS 5.1 digital camera. IHC, SR, and H&E slides were scanned using NanoZoomer-SQ Digital slide scanner (Hamamatsu Inc). The collagen proportional area was morphometrically quantified on SR-stained sections with image processing software (Image J, National Institutes of Health).

Collagen Stabilization Assay

To characterize and quantify the stability of the collagenous ECM, we performed stepwise collagen solubilization from livers using neutral salt (freshly secreted collagens and procollagens), acetic acid (more mature collagens), and acid pepsin (fibrillar, moderately cross-linked collagens) based on published protocols.[28,71] Briefly, 100 to 150 mg (0.10–0.15 gr) of snap frozen liver (4 samples per group, each pooled from pieces of 2–3 individual livers) was homogenized in 2 mL of neutral salt buffer (Tris Buffer) (0.5M NaCl, 0.05M Tris, pH 7.5, with Complete protease inhibitor [Roche]) and incubated at 4 °C overnight on a rotary shaker. After centrifugation at 24,000g for 30 minutes, the supernatant was collected for hydroxyproline determination. The

resulting pellet was extracted with 20 mL 0.5M acetic acid and incubated at 4 °C overnight on a rotary shaker. After centrifugation at 24.000g for 30 minutes, the supernatant was collected for hydroxyproline determination. To isolate pepsin soluble collagen, the resulted pellet was digested by pepsin (2 mg/mL in 0.5M acetic acid, fraction) at 4 °C overnight on a rotary shaker. After centrifugation at 24,000g for 30 minutes, the supernatant was collected for hydroxyproline (HYP) determination. The remaining insoluble fraction represents mature, highly cross-linked collagen. Collagen content solubilized in each extraction step, and the remaining insoluble collagen was quantified biochemically via HYP determination after completing acidic hydrolysis in 6N hydrochloric acid and expressed as the percentage of HYP recovered in all fractions.

Primary Mouse HSCs Isolation

Mouse livers were perfused with 10 mL of PBS and the 10 mL of collagenase type XI (0.25 mg/mL in HBSS [Sigma]) through the portal vein of euthanized adult (8–12 weeks) mice. The whole liver was then excised, cut into small pieces, and digested in 15 mL collagenase solution at 37°C for 30 minutes. Collagenase was inactivated by adding 10 mL cold HBSS containing 10% FBS. Collagenase was removed by 2 minutes of centrifugation at 1200g following 3× washing steps with cold HBSS followed by passing through a 70-μm nylon mesh. Next, primary mouse HSCs were purified from the total single cells. The pellet was resuspended in 10 mL of 35% Percoll (GE Healthcare, Pittsburgh, PA) with an overlay of 1 mL PBS. After centrifugation at 1130 g for 30 minutes (with no acceleration and no break speed), HSCs in the interphase layer between the PBS and Percoll were collected and washed with DMEM supplemented with 15% FBS. Cells were seeded in a 6-cm petri dish in pre-warmed DMEM (high glucose 4.5 g/L) (Gibco Thermofisher, Waltham, MA) supplemented with heat-inactivated 10% FBS (Sigma-Aldrich, St. Louis, MO), 1% penicillin/streptomycin (100 U/mL penicillin, 100 ug/mL streptomycin, Corning, NY), and sodium pyruvate (GibcoThermofisher). Isolated primary mouse HSCs were maintained at 37 °C, 5% CO2 in a humidified incubator.

Primary Monocyte Isolation From Bone Marrow

Bone marrow primary monocytes were isolated by flushing femurs and tibias of 8- to 10-week-old C57Bl/6

mice (Charles River Laboratories) with DMEM supplemented with 10% FBS, +1% penicillin/streptomycin, and 1% sodium pyruvate). Aggregates were mechanically dissociated by pipetting, and debris was removed by passaging the suspension through a 70-μm nylon mesh (Corning). Cells were washed twice with complete medium and seeded on 6-well ultra-low attachment surface plates (Corning) Cells were supplemented with 20 ng/mL rmM-CSF (R&D Systems, Minneapolis, MN) and cultured in a humidified incubator at 37 °C and 5% CO_2.

FITC-dextran Uptake Assay

To measure macrophage phagocytic ability, the FITC-dextran uptake assay was performed up by incubating cells with FITC-dextran. Briefly, macrophages were cultured on 24-well plates at a concentration of 5×10^4 cells/well. FITC-dextran was added into each well at a final concentration of 0.5 mg/mL, and the culture plates was incubated at 37 °C for 10 minutes. After incubation, wells were washed with PBS extensively to remove excess FITC-dextran. Cells then were fixed with paraformaldehyde 4% for 10 minutes. Cells were washed and nuclei were stained with DAPI.

Serum Marker Analysis

A cardiac terminal blood withdrawal was performed at the time of sacrifice. Blood was allowed to clot for 2 hours at room temperature before centrifugation at 2000 rpm for 10 minutes at 4 °C. Serum was isolated and stored at −80°C. Biochemical markers of liver injury were measured, including alkaline phosphatase, ALT, AST, total bilirubin, and albumin (DRI-CHEM 4000 Analyzer, Heska, Switzerland).

In vivo MRI and Image Analysis

Animals were anesthetized with 1% to 2% isoflurane with body temperature maintained at 37 °C. The tail vein was cannulated for intravenous delivery of contrast agent while the animal was positioned in the scanner in a custom-designed cradle. Imaging was performed at 4.7 T using a small-bore animal scanner (Bruker, Billerica, MA). Baseline axial and coronal 2D Fast Low Angle Shot images were acquired before and continuously for 30 minutes after injection of 0.2 mmol/kg Fe-PyC3A intravenously. Two-dimensional Fast Low Angle Shot image acquisition parameters were echo time/repetition time = 2.93/152 ms, flip angle = 60°, field of view = 33 × 33 mm, matrix = 140 × 140, and slice thickness = 1.0 mm. Data analysis included the calculation of CNR of the liver region of interest vs back muscle region of interest (ie, $CNR = \frac{S_{pancreas} - S_{Muscle}}{Stdev_{noise}}$). The differential (postinjection – preinjection) was further calculated and represented as delta CNR (dCNR).

Statistical Analysis

Results are expressed as the mean ± standard deviation. One-way analysis of variance followed by post-hoc Tukey tests with 2-tailed distribution were performed to analyze data among groups of 3 or more. The Student t test compared data between control and 1 experimental group. All statistical analyses were performed using either Graph-Pad Prism software (GraphPad Software, La Jolla, CA) or Intercooled Stata software, version 12.0 (StataCorp, College Station, TX).

References

1. Kisseleva T, Brenner D. Molecular and cellular mechanisms of liver fibrosis and its regression. Nat Rev Gastroenterol Hepatol 2021;18:151–166.
2. GBD 2017 Cirrhosis Collaborators. The global, regional, and national burden of cirrhosis by cause in 195 countries and territories, 1990-2017: a systematic analysis for the Global Burden of Disease Study 2017. Lancet Gastroenterol Hepatol 2020;5:245–266.
3. Drew L. Liver cirrhosis: scar wars. Nature 2018;564:S73.
4. Cao S, Liu M, Sehrawat TS, Shah VH. Regulation and functional roles of chemokines in liver diseases. Nat Rev Gastroenterol Hepatol 2021;18:630–647.
5. Puche JE, Saiman Y, Friedman SL. Hepatic stellate cells and liver fibrosis. Compr Physiol 2013;3:1473–1492.
6. Matsuda M, Seki E. Hepatic stellate cell-macrophage crosstalk in liver fibrosis and carcinogenesis. Semin Liver Dis 2020;40:307–320.
7. Miura K, Yang L, van Rooijen N, Ohnishi H, Seki E. Hepatic recruitment of macrophages promotes nonalcoholic steatohepatitis through CCR2. Am J Physiol Gastrointest Liver Physiol 2012;302:G1310–G1321.
8. Baeck C, Wei X, Bartneck M, Fech V, Heymann F, Gassler N, Hittatiya K, Eulberg D, Luedde T, Trautwein C, Tacke F. Pharmacological inhibition of the chemokine C-C motif chemokine ligand 2 (monocyte chemoattractant protein 1) accelerates liver fibrosis regression by suppressing Ly-6C(+) macrophage infiltration in mice. Hepatology 2014;59:1060–1072.
9. Matsuda M, Tsurusaki S, Miyata N, Saijou E, Okochi H, Miyajima A, Tanaka M. Oncostatin M causes liver fibrosis by regulating cooperation between hepatic stellate cells and macrophages in mice. Hepatology 2018; 67:296–312.
10. Wen Y, Lambrecht J, Ju C, Tacke F. Hepatic macrophages in liver homeostasis and diseases-diversity, plasticity and therapeutic opportunities. Cell Mol Immunol 2021;18:45–56.
11. Tacke F, Zimmermann HW. Macrophage heterogeneity in liver injury and fibrosis. J Hepatol 2014;60:1090–1096.
12. Li H, You H, Fan X, Jia J. Hepatic macrophages in liver fibrosis: pathogenesis and potential therapeutic targets. BMJ Open Gastroenterol 2016;3:e000079.
13. Bai L, Liu X, Zheng Q, Kong M, Zhang X, Hu R, Lou J, Ren F, Chen Y, Zheng S, Liu S, Han YP, Duan Z, Pandol SJ. M2-like macrophages in the fibrotic liver protect mice against lethal insults through conferring apoptosis resistance to hepatocytes. Sci Rep 2017;7: 10518.
14. Murray PJ, Wynn TA. Protective and pathogenic functions of macrophage subsets. Nat Rev Immunol 2011; 11:723–737.

15. Brune B, Dehne N, Grossmann N, Jung M, Namgaladze D, Schmid T, von Knethen A, Weigert A. Redox control of inflammation in macrophages. Antioxid Redox Signal 2013;19:595–637.

16. He C, Carter AB. The metabolic prospective and redox regulation of macrophage polarization. J Clin Cell Immunol 2015;6:371.

17. Soudi M, Zamocky M, Jakopitsch C, Furtmuller PG, Obinger C. Molecular evolution, structure, and function of peroxidasins. Chem Biodivers 2012;9:1776–1793.

18. Peterfi Z, Donko A, Orient A, Sum A, Prokai A, Molnar B, Vereb Z, Rajnavolgyi E, Kovacs KJ, Muller V, Szabo AJ, Geiszt M. Peroxidasin is secreted and incorporated into the extracellular matrix of myofibroblasts and fibrotic kidney. Am J Pathol 2009;175:725–735.

19. Ramachandran P, Dobie R, Wilson-Kanamori JR, Dora EF, Henderson BEP, Luu NT, Portman JR, Matchett KP, Brice M, Marwick JA, Taylor RS, Efremova M, Vento-Tormo R, Carragher NO, Kendall TJ, Fallowfield JA, Harrison EM, Mole DJ, Wigmore SJ, Newsome PN, Weston CJ, Iredale JP, Tacke F, Pollard JW, Ponting CP, Marioni JC, Teichmann SA, Henderson NC. Resolving the fibrotic niche of human liver cirrhosis at single-cell level. Nature 2019; 575:512–518.

20. Khan K, Rudkin A, Parry DA, Burdon KP, McKibbin M, Logan CV, Abdelhamed ZI, Muecke JS, Fernandez-Fuentes N, Laurie KJ, Shires M, Fogarty R, Carr IM, Poulter JA, Morgan JE, Mohamed MD, Jafri H, Raashid Y, Meng N, Piseth H, Toomes C, Casson RJ, Taylor GR, Hammerton M, Sheridan E, Johnson CA, Inglehearn CF, Craig JE, Ali M. Homozygous mutations in PXDN cause congenital cataract, corneal opacity, and developmental glaucoma. Am J Hum Genet 2011; 89:464–473.

21. Choi A, Lao R, Ling-Fung Tang P, Wan E, Mayer W, Bardakjian T, Shaw GM, Kwok PY, Schneider A, Slavotinek A. Novel mutations in PXDN cause microphthalmia and anterior segment dysgenesis. Eur J Hum Genet 2015;23:337–341.

22. Yan X, Sabrautzki S, Horsch M, Fuchs H, Gailus-Durner V, Beckers J, Hrabe de Angelis M, Graw J. Peroxidasin is essential for eye development in the mouse. Hum Mol Genet 2014;23:5597–5614.

23. Bhave G, Cummings CF, Vanacore RM, Kumagai-Cresse C, Ero-Tolliver IA, Rafi M, Kang JS, Pedchenko V, Fessler LI, Fessler JH, Hudson BG. Peroxidasin forms sulfilimine chemical bonds using hypohalous acids in tissue genesis. Nat Chem Biol 2012;8:784–790.

24. Tindall AJ, Pownall ME, Morris ID, Isaacs HV. Xenopus tropicalis peroxidasin gene is expressed within the developing neural tube and pronephric kidney. Dev Dyn 2005;232:377–384.

25. Zhang YS, He L, Liu B, Li NS, Luo XJ, Hu CP, Ma QL, Zhang GG, Li YJ, Peng J. A novel pathway of NADPH oxidase/vascular peroxidase 1 in mediating oxidative injury following ischemia-reperfusion. Basic Res Cardiol 2012;107:266.

26. Brown KL, Darris C, Rose KL, Sanchez OA, Madu H, Avance J, Brooks N, Zhang MZ, Fogo A, Harris R, Hudson BG, Voziyan P. Hypohalous acids contribute to renal extracellular matrix damage in experimental diabetes. Diabetes 2015;64:2242–2253.

27. Aycock RS, Seyer JM. Collagens of normal and cirrhotic human liver. Connect Tissue Res 1989;23:19–31.

28. Liu SB, Ikenaga N, Peng ZW, Sverdlov DY, Greenstein A, Smith V, Schuppan D, Popov Y. Lysyl oxidase activity contributes to collagen stabilization during liver fibrosis progression and limits spontaneous fibrosis reversal in mice. FASEB J 2016;30:1599–1609.

29. Bhave G, Colon S, Ferrell N. The sulfilimine cross-link of collagen IV contributes to kidney tubular basement membrane stiffness. Am J Physiol Renal Physiol 2017; 313:F596–F602.

30. Itoh M, Suganami T, Kato H, Kanai S, Shirakawa I, Sakai T, Goto T, Asakawa M, Hidaka I, Sakugawa H, Ohnishi K, Komohara Y, Asano K, Sakaida I, Tanaka M, Ogawa Y. CD11c+ resident macrophages drive hepatocyte death-triggered liver fibrosis in a murine model of nonalcoholic steatohepatitis. JCI Insight 2017;2:e92902.

31. Bertani FR, Mozetic P, Fioramonti M, Iuliani M, Ribelli G, Pantano F, Santini D, Tonini G, Trombetta M, Businaro L, Selci S, Rainer A. Classification of M1/M2-polarized human macrophages by label-free hyperspectral reflectance confocal microscopy and multivariate analysis. Sci Rep 2017;7:8965.

32. Shan Z, Ju C. Hepatic macrophages in liver injury. Front Immunol 2020;11:322.

33. Kessenbrock K, Plaks V, Werb Z. Matrix metalloproteinases: regulators of the tumor microenvironment. Cell 2010;141:52–67.

34. Siller-Lopez F, Sandoval A, Salgado S, Salazar A, Bueno M, Garcia J, Vera J, Galvez J, Hernandez I, Ramos M, Aguilar-Cordova E, Armendariz-Borunda J. Treatment with human metalloproteinase-8 gene delivery ameliorates experimental rat liver cirrhosis. Gastroenterology 2004;126:1122–1133, discussion: 949.

35. Endo H, Niioka M, Sugioka Y, Itoh J, Kameyama K, Okazaki I, Ala-Aho R, Kahari VM, Watanabe T. Matrix metalloproteinase-13 promotes recovery from experimental liver cirrhosis in rats. Pathobiology 2011; 78:239–252.

36. Fallowfield JA, Mizuno M, Kendall TJ, Constandinou CM, Benyon RC, Duffield JS, Iredale JP. Scar-associated macrophages are a major source of hepatic matrix metalloproteinase-13 and facilitate the resolution of murine hepatic fibrosis. J Immunol 2007;178:5288–5295.

37. Berg JT, Lee ST, Thepen T, Lee CY, Tsan MF. Depletion of alveolar macrophages by liposome-encapsulated dichloromethylene diphosphonate. J Appl Physiol (1985) 1993;74:2812–2819.

38. Lehenkari PP, Kellinsalmi M, Napankangas JP, Ylitalo KV, Monkkonen J, Rogers MJ, Azhayev A, Vaananen HK, Hassinen IE. Further insight into mechanism of action of clodronate: inhibition of mitochondrial ADP/ATP translocase by a nonhydrolyzable, adenine-

containing metabolite. Mol Pharmacol 2002; 61:1255–1262.

39. Borst K, Frenz T, Spanier J, Tegtmeyer PK, Chhatbar C, Skerra J, Ghita L, Namineni S, Lienenklaus S, Koster M, Heikenwaelder M, Sutter G, Kalinke U. Type I interferon receptor signaling delays Kupffer cell replenishment during acute fulminant viral hepatitis. J Hepatol 2018; 68:682–690.

40. Bleriot C, Dupuis T, Jouvion G, Eberl G, Disson O, Lecuit M. Liver-resident macrophage necroptosis orchestrates type 1 microbicidal inflammation and type-2-mediated tissue repair during bacterial infection. Immunity 2015;42:145–158.

41. Li M, Lai X, Zhao Y, Zhang Y, Li M, Li D, Kong J, Zhang Y, Jing P, Li H, Qin H, Shen L, Yao L, Li J, Dou K, Zhang J. Loss of NDRG2 in liver microenvironment inhibits cancer liver metastasis by regulating tumor associate macrophages polarization. Cell Death Dis 2018;9:248.

42. Matsumoto M, Hada N, Sakamaki Y, Uno A, Shiga T, Tanaka C, Ito T, Katsume A, Sudoh M. An improved mouse model that rapidly develops fibrosis in non-alcoholic steatohepatitis. Int J Exp Pathol 2013; 94:93–103.

43. Li L, Duan M, Chen W, Jiang A, Li X, Yang J, Li Z. The spleen in liver cirrhosis: revisiting an old enemy with novel targets. J Transl Med 2017;15:111.

44. Ramachandran P, Pellicoro A, Vernon MA, Boulter L, Aucott RL, Ali A, Hartland SN, Snowdon VK, Cappon A, Gordon-Walker TT, Williams MJ, Dunbar DR, Manning JR, van Rooijen N, Fallowfield JA, Forbes SJ, Iredale JP. Differential Ly-6C expression identifies the recruited macrophage phenotype, which orchestrates the regression of murine liver fibrosis. Proc Natl Acad Sci U S A 2012;109:E3186–E3195.

45. Tsuchida T, Friedman SL. Mechanisms of hepatic stellate cell activation. Nat Rev Gastroenterol Hepatol 2017; 14:397–411.

46. Iyer SS, Cheng G. Role of interleukin 10 transcriptional regulation in inflammation and autoimmune disease. Crit Rev Immunol 2012;32:23–63.

47. Zhang DY, Goossens N, Guo J, Tsai MC, Chou HI, Altunkaynak C, Sangiovanni A, Iavarone M, Colombo M, Kobayashi M, Kumada H, Villanueva A, Llovet JM, Hoshida Y, Friedman SL. A hepatic stellate cell gene expression signature associated with outcomes in hepatitis C cirrhosis and hepatocellular carcinoma after curative resection. Gut 2016;65:1754–1764.

48. Wen G, Zhang C, Chen Q, Luong le A, Mustafa A, Ye S, Xiao Q. A novel role of matrix metalloproteinase-8 in macrophage differentiation and polarization. J Biol Chem 2015;290:19158–19172.

49. Wang C, Yu X, Cao Q, Wang Y, Zheng G, Tan TK, Zhao H, Zhao Y, Wang Y, Harris D. Characterization of murine macrophages from bone marrow, spleen and peritoneum. BMC Immunol 2013;14:6.

50. Ma QL, Zhang GG, Peng J. Vascular peroxidase 1: a novel enzyme in promoting oxidative stress in cardiovascular system. Trends Cardiovasc Med 2013; 23:179–183.

51. Wang H, Jordan VC, Ramsay IA, Sojoodi M, Fuchs BC, Tanabe KK, Caravan P, Gale EM. Molecular magnetic resonance imaging using a redox-active iron complex. J Am Chem Soc 2019;141:5916–5925.

52. Koyama Y, Brenner DA. New therapies for hepatic fibrosis. Clin Res Hepatol Gastroenterol 2015;39(Suppl 1):S75–S79.

53. Poli G, Leonarduzzi G, Biasi F, Chiarpotto E. Oxidative stress and cell signalling. Curr Med Chem 2004; 11:1163–1182.

54. Lazar E, Peterfi Z, Sirokmany G, Kovacs HA, Klement E, Medzihradszky KF, Geiszt M. Structure-function analysis of peroxidasin provides insight into the mechanism of collagen IV crosslinking. Free Radic Biol Med 2015; 83:273–282.

55. Colon S, Bhave G. Proprotein convertase processing enhances peroxidasin activity to reinforce collagen IV. J Biol Chem 2016;291:24009–24016.

56. Liu Z, Xu Q, Yang Q, Cao J, Wu C, Peng H, Zhang X, Chen J, Cheng G, Wu Y, Shi R, Zhang G. Vascular peroxidase 1 is a novel regulator of cardiac fibrosis after myocardial infarction. Redox Biol 2019;22:101151.

57. Costas L, Herz CT, Hobaus C, Koppensteiner R, Schernthaner GH. Vascular peroxidase 1 is independently associated with worse kidney function in patients with peripheral artery disease. J Nephrol 2021; 34:165–172.

58. Fidler AL, Vanacore RM, Chetyrkin SV, Pedchenko VK, Bhave G, Yin VP, Stothers CL, Rose KL, McDonald WH, Clark TA, Borza DB, Steele RE, Ivy MT, Aspirnauts, Hudson JK, Hudson BG. A unique covalent bond in basement membrane is a primordial innovation for tissue evolution. Proc Natl Acad Sci U S A 2014;111:331–336.

59. Arteel GE, Naba A. The liver matrisome - looking beyond collagens. JHEP Rep 2020;2(4):100115.

60. Soucie EL, Weng Z, Geirsdottir L, Molawi K, Maurizio J, Fenouil R, Mossadegh-Keller N, Gimenez G, VanHille L, Beniazza M, Favret J, Berruyer C, Perrin P, Hacohen N, Andrau JC, Ferrier P, Dubreuil P, Sidow A, Sieweke MH. Lineage-specific enhancers activate self-renewal genes in macrophages and embryonic stem cells. Science 2016;351(6274):aad5510.

61. Heymann F, Hammerich L, Storch D, Bartneck M, Huss S, Russeler V, Gassler N, Lira SA, Luedde T, Trautwein C, Tacke F. Hepatic macrophage migration and differentiation critical for liver fibrosis is mediated by the chemokine receptor C-C motif chemokine receptor 8 in mice. Hepatology 2012;55:898–909.

62. Lo RC, Kim H. Histopathological evaluation of liver fibrosis and cirrhosis regression. Clin Mol Hepatol 2017; 23:302–307.

63. Brempelis KJ, Crispe IN. Infiltrating monocytes in liver injury and repair. Clin Transl Immunology 2016;5:e113.

64. Scott CL, Zheng F, De Baetselier P, Martens L, Saeys Y, De Prijck S, Lippens S, Abels C, Schoonooghe S, Raes G, Devoogdt N, Lambrecht BN, Beschin A, Guilliams M. Bone marrow-derived monocytes give rise to self-renewing and fully differentiated Kupffer cells. Nat Commun 2016;7:10321.

65. Heymann F, Peusquens J, Ludwig-Portugall I, Kohlhepp M, Ergen C, Niemietz P, Martin C, van Rooijen N, Ochando JC, Randolph GJ, Luedde T, Ginhoux F, Kurts C, Trautwein C, Tacke F. Liver inflammation abrogates immunological tolerance induced by Kupffer cells. Hepatology 2015;62:279–291.

66. Xi S, Zheng X, Li X, Jiang Y, Wu Y, Gong J, Jie Y, Li Z, Cao J, Sha L, Zhang M, Chong Y. Activated hepatic stellate cells induce infiltration and formation of CD163(+) macrophages via CCL2/CCR2 pathway. Front Med (Lausanne) 2021;8:627927.

67. Kruger AJ, Fuchs BC, Masia R, Holmes JA, Salloum S, Sojoodi M, Ferreira DS, Rutledge SM, Caravan P, Alatrakchi N, Vig P, Lefebvre E, Chung RT. Prolonged cenicriviroc therapy reduces hepatic fibrosis despite steatohepatitis in a diet-induced mouse model of nonalcoholic steatohepatitis. Hepatol Commun 2018; 2:529–545.

68. Hanmer KL, Mavri-Damelin D. Peroxidasin is a novel target of the redox-sensitive transcription factor Nrf2. Gene 2018;674:104–114.

69. Fuchs BC, Hoshida Y, Fujii T, Wei L, Yamada S, Lauwers GY, McGinn CM, DePeralta DK, Chen X, Kuroda T, Lanuti M, Schmitt AD, Gupta S, Crenshaw A, Onofrio R, Taylor B, Winckler W, Bardeesy N, Caravan P, Golub TR, Tanabe KK. Epidermal growth factor receptor inhibition attenuates liver fibrosis and development of hepatocellular carcinoma. Hepatology 2014; 59:1577–1590.

70. Erstad DJ, Sojoodi M, Taylor MS, Jordan VC, Farrar CT, Axtell AL, Rotile NJ, Jones C, Graham-O'Regan KA, Ferreira DS, Michelakos T, Kontos F, Chawla A, Li S, Ghoshal S, Chen YI, Arora G, Humblet V, Deshpande V, Qadan M, Bardeesy N, Ferrone CR, Lanuti M, Tanabe KK, Caravan P, Fuchs BC. Fibrotic response to neoadjuvant therapy predicts survival in pancreatic cancer and is measurable with collagen-targeted molecular MRI. Clin Cancer Res 2020;26:5007–5018.

71. Popov Y, Sverdlov DY, Sharma AK, Bhaskar KR, Li S, Freitag TL, Lee J, Dieterich W, Melino G, Schuppan D. Tissue transglutaminase does not affect fibrotic matrix stability or regression of liver fibrosis in mice. Gastroenterology 2011;140:1642–1652.

Correspondence
Address correspondence to: Kenneth K. Tanabe, Division of Gastrointestinal and Oncologic Surgery, Massachusetts General Hospital, 55 Fruit St, Boston, MA 02114. e-mail: ktanabe@partners.org; tel: (617) 724-3868.